Second Order Macroscopic Traffic Flow Model Validation Using Automatic Differentiation with Resilient Backpropagation and Particle Swarm Optimisation Algorithms

Adam Poole and Apostolos Kotsialos*
e-mail: {a.j.poole,apostolos.kotsialos}@durham.ac.uk
**corresponding author*

School of Engineering and Computing Sciences, Durham University
Stockton Road, DH1 3LE, Durham, United Kingdom

Abstract

The problem of validating the Modéle d'Écoulement de Trafic sur Autoroute NETworks (METANET) model of a motorway section is considered. Model calibration is formulated as a least squares error minimisation problem with explicit penalisation of fundamental diagram parameter variation. The Automatic Differentiation by Overloading in C++ (ADOL-C) library is incorporated into the METANET source code and is coupled with the Resilient Back Propagation (RPROP) heuristic for solving the minimisation problem. The result is a very efficient system which is able to be calibrate METANET by determining the density and speed equation parameters as well as the fundamental diagrams used. Information obtained from the system's Jacobian provides extra insight into the dynamics showing how sensitivities propagate into the network. A 22 km site near Sheffield, UK, using data from three different days is considered. In addition to the ADOL-C/RPROP system, three particle swarm optimisation algorithms are used for solving the calibration problem. In all cases, the optimal parameter sets found are verified on data not used during calibration. Although, all three sets of data display a similar congestion pattern, the verification process showed that only one of them is capable of leading to parameter sets that capture the underlying dynamics of the traffic flow process.

Keywords: Traffic flow models, parameter estimation, resilient back

propagation, automatic differentiation, particle swarm optimisation.

---

1. Introduction and Background

The macroscopic description of traffic along a motorway was introduced in the seminal papers of Lighthill and Whitham (1955) and Richards (1956), resulting to the LWR model relating the density ρ and flow q at location s and time t

$$\frac{\partial \rho(s,t)}{\partial t} + \frac{\partial q(s,t)}{\partial s} = 0. \tag{1}$$

The nonlinear relationship between flow and density is

$$q(s,t) = \rho(s,t) V\left[\rho(s,t)\right] \tag{2}$$

where $V\left[\rho(s,t)\right]$ (km/h) is the equilibrium relationship between density and mean speed, i.e. the Fundamental Diagram (FD) of traffic. For any given site a number of FD may be used reflecting changes in the number of lanes and road geometry, bottleneck locations and significant gradient variability.

Typically, a space and time discretised version of eqn. (1), along with the FD constitute the basic elements of a first order macroscopic traffic flow model, see e.g. (Lighthill and Whitham, 1955; Richards, 1956; Daganzo, 1994).

Payne-Whitham type second order models result from coupling eqn. (1) with an empirical equation governing the mean speed $v(x,t)$ dynamics (Payne, 1971; Whitham, 1974), with the form

$$\frac{\partial v(s,t)}{\partial t} + v(s,t)\frac{\partial v(s,t)}{\partial s} + \frac{1}{\rho(s,t)}\frac{\partial P(s,t)}{\partial s} = \frac{1}{\tau}\left\{V\left[\rho(s,t)\right] - v(s,t)\right\} \tag{3}$$

where τ is a relaxation constant and $P(s,t)$ a pressure term, which gives rise to a range of different models of this family, (Helbing et al., 2002).

Irrespective of the model's order, a number of parameters characterising the aggregate infrastructure-vehicle-driver behaviour are used. Using data sets of traffic counts and vehicle speeds, typically obtained by means of inductive loop detectors embedded in the motorway, a rigorous model validation procedure needs to take place, for identifying an optimal set of parameters. This procedure is performed in two steps, calibration and verification. Calibration requires the solution of an error minimisation problem and verification involves testing the solutions obtained on data that were not

used for furnishing the corresponding calibration optimisation problem. This paper is concerned with model validation of a traffic flow model along the lines given in (Cremer and Papageorgiou, 1981) and (Papageorgiou, 1983).

First order traffic flow model calibration is concerned mostly with determining the FD parameters of discrete road sections, depending on the discretisation scheme used for (1). The most commonly used model of this order is the Cell Transmission Model (CTM) by Daganzo (1994) and detailed calibration efforts may be found in (Munoz et al., 2006, 2004).

A comparative study of the CTM and the second order Modéle d'Écoulement de Trafic sur Autoroute NETworks (METANET) by Messmer and Papageorgiou (1990) for a motorway in Greece based on the Nelder-Mead algorithm (Nelder and Mead, 1965) is provided by Spiliopoulou et al. (2014).

An extensive validation study of METANET, using a source code different than the one employed here, for the Paris ring road is reported by Papageorgiou et al. (1990). The METANET validation of the large scale network of the Amsterdam orbital motorways is described in (Kotsialos et al., 2002, 1998). In (Frejo et al., 2012) a METANET model parameter identification algorithm is discussed using data from a 4.65 km stretch of a California highway; the original expression used for FD in METANET is replaced with a two-regime model and the resulting optimisation problem is solved using a sequential quadratic programming algorithm.

A linear varying parameter method is described by Luspay et al. (2010, 2011, 2009) for identifying second order model parameters. A simultaneous perturbation stochastic approximation method is used by Alessandri et al. (2006) for the same purpose using information from mobile phones. In (Treiber and Kesting, 2012) a method calculating the model parameters by comparing the congestion pattern of the data and model output aiming at avoiding incorrect data forms, was used. The model used by Treiber and Kesting (2012) is validated by Ngoduy and Maher (2012) on a 10km section of a UK highway.

As is mentioned by Ngoduy and Maher (2012), the optimisation problem related to model calibration has numerous local minima. Hence, efficient optimisation algorithms need to be used for obtaining parameter sets that make models capable of representing traffic dynamics. Most of the proposed, if not all, algorithms used are population based derivative free methods, employing direct or stochastic search. In a recent overview of nonlinear programming methods used for macroscopic traffic flow model calibration by Kontorinaki et al. (2015), gradient based optimisation algorithms are not

considered as a viable option due to the nonlinear and non-convex nature of the least-squares optimization problem. However, it is shown here that a simple globalisation strategy based on a multistart scheme of a gradient based heuristic is capable of efficiently solving this problem.

For the modelling of the Paris and Amsterdam sites discussed by Papageorgiou et al. (1990); Kotsialos et al. (2002, 1998), the deterministic search algorithm of Box (1965) was used. A cross entropy method is used by Ngoduy and Maher (2012). A simplex based algorithm was used by Ngoduy et al. (2004) to validate various numerical schemes used for solving the macroscopic model equations. A number of population based derivative free optimisation algorithms used for calibration are discussed by Spiliopoulou et al. (2015).

A nonlinear mixed integer optimisation formulation was introduced for the macroscopic traffic flow model calibration problem which was solved by means of a genetic algorithm by Poole and Kotsialos (2012). METANET was treated as a simulation black box. An additional requirement introduced was the automatic spatial assignment, i.e. determination of the location and extension, of fundamental diagrams (FD). The motivation behind this is that current calibration practice either uses expert engineering opinion to make a decision about the FD or use a separate FD for every discrete road segment. In the first case, intuition, past experience, visual inspection and preliminary data analysis result to an *ad-hoc* approach leading away from systems that embed knowledge in their own structure and the display of more intelligent forms of automation, (Kotsialos and Poole, 2013, 2016). In the latter case, overparametrisation is a clear risk since typically three parameters are necessary for defining a FD.

The problem formulation suggested by Poole and Kotsialos (2012) allows the selection of FD location for homogeneous road stretches, which themselves are split into segments. It also penalises the variance between their parameters. The rationale behind this penalisation is that by treating the FD as an extensive quantity whose start and end are decision variables in an optimisation problem, the parameter variance penalty will result to solutions that favour similar FD. This kind of similarity was employed as guidance when validating the large scale model of the Amsterdam motorway networks, (Kotsialos et al., 1998, 2002).

A more detailed calibration work using classic and recent variants of particle swarm optimisation (PSO) and cuckoo search algorithms is reported by Poole and Kotsialos (2016). These evolutionary algorithms (EA) were used for calibrating a site near Heathrow Airport and a site near Sheffield,

UK. Optimal parameters were determined capturing the essential characteristics of the underlying traffic dynamics as was shown in the ensuing model verification. In total, ten different EA, seven variations of particle swarm optimisation (PSO), two of cuckoo search and a simple genetic algorithm acting as a baseline, were considered by Poole and Kotsialos (2016). One of the main conclusions drawn regarding algorithmic performance, was that the PSO family of algorithms outperformed the cuckoo search and genetic algorithm; interestingly it was one of the simplest types of PSO, a variant called Local PSO (LPSO) (Kennedy and Mendes, 2002), that proved to be the more efficient among the PSO variants, in terms of number of iterations and error. Based on the analysis of Poole and Kotsialos (2016), three PSO algorithms were selected for this paper.

One of this paper's original contributions is providing the details of a gradient based optimisation method for solving the calibration problem. Extra information that becomes available from the process of calculating partial derivatives is highlighted as well. The gradient calculation is performed by use of the automatic differentiation (AD) software ADOL-C, (Walther and Griewank, 2012). AD software technology is used for avoiding hard-coding analytic expressions of the gradient vector. ADOL-C performs these calculations based on the computation source code without resorting to perturbations, which require multiple objective function evaluations, and therefore a lot of simulation runs, for approximating partial derivatives. The full set of the necessary derivatives is obtained by a single simulation run. This allows the development of the space-distance diagrams of the model's sensitivity.

The resilient backpropagation (RPROP) heuristic (Riedmiller and Braun, 1993) is the optimisation scheme used for utilising the calculated partial derivatives. RPROP is capable of solving non linear, non smooth and non convex problems, and is equally efficient if not superior to more sophisticated optimisation approaches, as demonstrated by Kotsialos (2013, 2014). Only one evaluation of the gradient vector per iteration is required, as opposed to other line search and trust region methods (Nocedal and Wright, 2006; Fletcher, 2013). It is robust in view of errors in the partial derivatives' calculation since it does not make explicit use of their values but of their sign. Errors in the partial derivatives' calculation can be tolerated as long as their sign is correct.

The work presented here differs from what is reported in (Poole and Kotsialos, 2016) at three main points. First, a slightly different objective function is used here, where only the space mean speed error is considered

explicitly as opposed to a total error of weighted flow and mean speed errors. Second, only evolutionary algorithms are considered there. Here, the best performing ones are presented next to the gradient based heuristic algorithm RPROP. Third, the system architecture of the population based optimisation discussed in (Poole and Kotsialos, 2016) does not require any change in the source code of the METANET simulator; it is a more modular design which avoids source code intervention. The integration of the ADOL-C software technology with macroscopic traffic flow simulation and the RPROP heuristic is one of the main novel contributions of this paper.

Although the use of AD results to an increase of the computation overhead, compared to the use of analytical expressions for the partial derivatives, the resulting iterative scheme in its multistart version still outperforms evolutionary based approaches. Long convergence times are not necessarily a drawback for the operational time scales of a model validation application. Such an application hosted within the information infrastructure ecosystem of a traffic control centre would face relatively large time scales to operate. A well-calibrated model can remain valid for several months before becoming obsolete due to data ageing. This allows a modelling application to follow a "rest and digest" policy collecting and processing streams of data from the surveillance database. Periodic updates and evaluation of optimisation solvers' performance can be part of a self-managing modelling application maintaining model relevance, (Kotsialos and Poole, 2013, 2016).

The rest of this paper is organised as follows. Section 2 provides an overview of the METANET model. The calibration problem formulation is discussed in 3. The optimisation algorithms used and developed for this paper are described in 4 along with their implementation. Section 5 provides the details of the site and available data. The calibration process and results are discussed in 6 and the verification of the obtained solution in Section 7. Section 8 concludes this paper and an outline of future research is given as well.

2. METANET Model Overview

The METANET simulator is a discrete form of Payne's model (3) and is able to model arbitrary motorway networks of any topology. A network is represented as a directed graph consisting of nodes and links. Links represent homogeneous road sections, where the number of lanes is a constant and there is no significant change of geometry, curvature or gradient. Furthermore, no

traffic sources or sinks (junctions) exist within a link. Nodes connect links and are used at places where the geometry of the motorway changes or at on-/off-ramp junctions. Each node has at least one incoming and one outgoing link. Traffic enters via origin links and leaves through destination links.

Time is discretised globally by a time step T and there are K steps in the time horizon. Each motorway link m is discretised into N_m segments of equal length L_m as shown in Figure 1. The traffic conditions in segment i of link m, at time instant $t = kT$, $k = 0, 1, \ldots, K$, described by the density $\rho_{m,i}(k)$ (veh/km/lane), the mean speed $v_{m,i}(k)$ (km/h) and the traffic flow $q_{m,i}(k)$ (veh/h).

[Figure 1 about here.]

By discretising equations (1) and (3), (Papageorgiou et al., 1990; Messmer and Papageorgiou, 1990; METANET, 2008), the discrete time motorway traffic flow model is the following.

$$\rho_{m,i}(k+1) = \rho_{m,i}(k) + \frac{T}{L_m \lambda_m}[q_{m,i-1}(k) - q_{m,i}(k)] \tag{4}$$

$$q_{m,i}(k) = \rho_{m,i}(k) v_{m,i}(k) \lambda_m \tag{5}$$

$$\begin{aligned} v_{m,i}(k+1) &= v_{m,i}(k) + \frac{T}{\tau}\{V[\rho_{m,i}(k)] - v_{m,i}(k)\} \\ &\quad + \frac{T}{L_m} v_{m,i}(k)[v_{m,i-1}(k) - v_{m,i}(k)] \\ &\quad - \frac{\nu T}{\tau L_m} \frac{\rho_{m,i+1}(k) - \rho_{m,i}(k)}{\rho_{m,i}(k) + \kappa} \end{aligned} \tag{6}$$

where λ_m is the number of lanes of link m, ν an anticipation constant and κ a numerical stability constant. The FD functional expression used is

$$V[\rho_{m,i}(k)] = v_{f,m} \cdot \exp\left[-\frac{1}{\alpha_m}\left(\frac{\rho_{m,i}(k)}{\rho_{cr,m}}\right)^{\alpha_m}\right] \tag{7}$$

where $\rho_{cr,m}$ is the critical density of link m and α_m a parameter. Parameters $v_{f,m}$, $\rho_{cr,m}$, α_m, define a link's FD.

In order to account for speed drops due to on-ramp inflow and merging phenomena the term $-\delta T q_\mu(k) v_{m,1}(k)/(L_m \lambda_m(\rho_{m,1}(k) + \kappa))$ is added at the

right hand side of (6), where δ a constant, μ the merging link and m the leaving link. This term is included only when the speed equation is applied to the first segment of the downstream link m. Speed decreases due to weaving are accounted for by adding the term $-\phi T \Delta\lambda \rho_{m,N_m}(k) v_{m,N_m}(k)^2/(L_m \lambda_m \rho_{cr,m})$ to the right hand side of (6), where $\Delta\lambda$ is the reduction in the number of lanes and ϕ another parameter. This term is only applied to the last segment of the link upstream of a lane drop.

METANET employs a simple queuing model for collecting the demand during period k at origin o, and subsequently forwarding it into the mainstream. This is used for the calculation of the origin link's o outflow $q_o(k)$ into the motorway. However, for the model validation problem, $q_o(k)$ is a direct measurement from the loop detectors. Hence, the queueing model is bypassed, since the measurement is directly fed into the model and there is no need for it.

In order for the speed equation to be applied at every exit location s, the density trajectories $\rho_s(k)$ are provided as boundary conditions over the time horizon.

Finally, a node model is used to assign flows at motorway junctions. Let I_n and O_n denote the set of incoming and outgoing links to and from, respectively, node n. Then the sum of all flow entering the node n during time period k, $Q_n(k)$ is given by

$$Q_n(k) = \sum_{\mu \in I_n} q_{\mu,N_\mu}(k) \quad \forall n. \tag{8}$$

The turning rate $\beta_n^m(k)$ is defined as the percentage of $Q_n(k)$ leaving through out link $m \in O_n$ during period k. $q_{m,0}(k)$ required by eqn. (4) when $i = 1$ is calculated from

$$q_{m,0}(k) = \beta_n^m(k) \cdot Q_n(k) \quad \forall m \in O_n. \tag{9}$$

For a full description of the METANET, see (Messmer and Papageorgiou, 1990) or Appendix A of (METANET, 2008).

By substituting (5), (8), (9) into (4) and the calculation of mean speeds and densities acting over nodes into (6) the model can be expressed in the following discrete dynamic state-space form

$$\mathbf{x}(k+1) = \mathbf{f}\left[\mathbf{x}(k), \mathbf{d}(k); \mathbf{z}\right]. \tag{10}$$

The state vector is

$$\mathbf{x} = \left[\rho_{1,1}\, v_{1,1} \ldots \rho_{1,N_1}\, v_{1,N_1} \ \ldots \rho_{M_1,1}\, v_{M_1,1} \ \ldots \rho_{M_1,N_{M_1}}\, v_{M_1,N_{M_1}}\right]^T \tag{11}$$

where M_1 is the number of motorway links in the network.

The disturbance vector $\mathbf{d}$ consists of the inflows q_o entering the system from entry points (origin links) and optionally their speeds v_o; the densities ρ_s at the destination links; and the turning rates at every split junction. These quantities are organised into vector

$$\mathbf{d} = \left[q_1\, v_1\, \ldots q_{M_2}\, v_{M_2} \rho_1 \ldots \rho_{M_3}\, \beta_1^{\mu_1} \ldots \beta_{M_4}^{\mu_{M_4}}\right]^T \tag{12}$$

where M_2 is the number of origins, M_3 the number of destinations, M_4 the number of split junctions and $\mu_n \in O_n$ the index of the destination link sending flow out of the system at node n.

Vector $\mathbf{z}$ consists of the model parameters as encountered in the dynamic density (4), speed (6) and fundamental diagram (7) equations. It includes the network-wide global parameters $\rho_{\max}$, $v_{\min}$, τ, ν, ϕ, δ and κ. It also contains parameters related to the fundamental diagram, i.e. v_f, α and ρ_{cr} for each FD used.

3. The Calibration Optimisation Problem Formulation

From a known initial state $\mathbf{x}_0$ and known disturbance trajectories $\mathbf{d}(k)$, $k = 0, \ldots, K-1$, a forward integration of (10) results to a full profile of the traffic conditions over the time horizon. A set of measurements $\mathbf{y}$ from a number of locations along the motorway, is used for comparing reality with model output. The error minimisation problem takes the form

$$\min_{\mathbf{z}} J\left[\mathbf{x}(k), \mathbf{y}(k)\right] \tag{13}$$

subject to

$$\mathbf{x}(k+1) = \mathbf{f}\left[\mathbf{x}(k), \mathbf{d}(k); \mathbf{z}\right],\ \mathbf{x}(0) = \mathbf{x}_0 \tag{14}$$

$$\mathbf{z}_{\min} \leq \mathbf{z} \leq \mathbf{z}_{\max} \tag{15}$$

where $J\left[\mathbf{x}(k), \mathbf{y}(k)\right]$ is the error function and $\mathbf{z}_{\min}$ and $\mathbf{z}_{\max}$ are the lower and upper bounds, respectively, of $\mathbf{z}$'s elements. The evaluation of J for a particular value of $\mathbf{z}$ requires the forward integration of (14) given as input the measured $\mathbf{x}_0$ and $\mathbf{d}(k)$.

The parameter vector $\mathbf{z}$ consists of two parts, the global parameters and those defining the FD used. Prior to the solution of problem (13)–(15), there has to be a decision based on knowledge of the network's congestion dynamics

related to the number of FDs to be used and for each one the list of motorway links using them.

Let $\widehat{N}$ be the number of FDs used; each ones' parameters ρ_{cr}, α and v_f need to be included in $\mathbf{z}$, which takes the form

$$\mathbf{z} = \left[\tau\, \kappa\, \nu\, \rho_{\max}\, v_{\min}\, \delta\, \phi\, v_f^1\, \alpha^1\, \rho_{cr}^1\, \ldots v_f^{\widehat{N}}\, \alpha^{\widehat{N}}\, \rho_{cr}^{\widehat{N}}\right]^T. \tag{16}$$

When $\widehat{N} = 1$ then a single fundamental diagram is used for the site. If $\widehat{N} = M_1$ then every link has its own FD.

The minimal use of FDs can either be explicitly enforced by introducing an inequality constraint or be implicitly penalised in the objective function. If the first option is followed, then $\mathbf{z}$ needs to be restructured to allow for this constraint to be expressed.

Let l^ℓ be the number of links FD ℓ is applied to, i.e. its spatial limitation. The revised vector of model parameters is

$$\mathbf{z} = \left[\tau\, \kappa\, \nu\, \rho_{\max}\, v_{\min}\, \delta\, \phi\, v_f^1\, \alpha^1\, \rho_{cr}^1\, l^1 \ldots v_f^{\widehat{N}}\, \alpha^{\widehat{N}}\, \rho_{cr}^{\widehat{N}}\, l^{\widehat{N}}\right]^T \tag{17}$$

where $l^\ell \in [0, M_1]$, $\ell = 1, \ldots, \widehat{N}$. The evolutionary algorithms used by Poole and Kotsialos (2016) for solving problem (13)–(15) use the form of $\mathbf{z}$ given in (17) and more details on the method can be found there. However, the requirement of specifying the spatial extension of an FD in terms of the links defined in the METANET network description file requires the introduction of the integer decision variable l^ℓ that creates problems in the calculation of partial derivatives. The variable l^ℓ provides a mapping to the links' list that cannot be differentiated.

Such a complication does not create a significant problem for population based methods. Therefore, for the EA used here, $\mathbf{z}$ has the form given in (17). For the gradient based optimisation method $\mathbf{z}$ has the form given by (16) and $\widehat{N} = M_1$. In both cases, the parameters' upper and lower bounds in (15) are given by Table 1. Irrespective of which of the two is used, $\mathbf{z}$'s dimension is denoted as Γ.

[Table 1 about here.]

Let us assume that there are M_5 loop detectors on the motorway providing flow and speed measurements. As observed by Spiliopoulou et al. (2014), the

flow and speed errors are not antagonistic in the sense that if the model mean speed given by (6) is correct then the flow will also be correct by virtue of the density equation (4). Hence, the measurements vector used for calculating the error term in the objective function includes only speeds and takes the form

$$\mathbf{y} = [y_{1,v} \cdots y_{M_5,v}]^T \tag{18}$$

where $y_{j,v}$ is the space mean speed from sensor j, $j = 1, \ldots, M_5$.

A global list is retained assigning each sensor to the corresponding motorway link it belongs to. If sensor j is installed at segment i_j of link m_j, then the discrepancy between $y_{j,v}(k)$ and $v_{m_j,i_j}(k)$ gives a measure of the model's accuracy. Typically, the sensors' measurement sample time T_s is larger than the model sample time T. For example, for the data used here, $T_s = 60$ seconds whereas $T = 8$ seconds. For each model time period k the measurement sample period it belongs to is identified and the model outputs are compared to the same set of measurements.

Measurement location j's contribution to the speed square error terms is given by

$$E_{j,v}\left[\mathbf{x}(k), \mathbf{y}(k)\right] = \left[y_{j,v}(k) - v_{m_j,i_j}(k)\right]^2. \tag{19}$$

The total error over the whole network and time horizon is given by the expression

$$J_v\left[\mathbf{x}(k), \mathbf{y}(k)\right] = \frac{1}{KM_5} \sum_{k=1}^{K} \sum_{j=1}^{M_5} E_{j,v}\left[\mathbf{x}(k), \mathbf{y}(k)\right]. \tag{20}$$

In order to implicitly achieve more relevant assignments of FD the following penalty term $J_p(\mathbf{z})$ is included in the objective function.

$$J_p(\mathbf{z}) = \sum_{\ell=1}^{\widehat{N}-1} \sum_{r=\ell+1}^{\widehat{N}} \left[w_v \left(v_f^\ell - v_f^r\right)^2 + w_\rho \left(\rho_{cr}^\ell - \rho_{cr}^r\right)^2 + w_\alpha \left(\alpha^\ell - \alpha^r\right)^2 \right] \tag{21}$$

where w_v, w_ρ and w_α are weighting parameters and are set to 0.001, 0.0015 and 1.0, respectively. This term considers all combinations of different FD used for a site and penalises large variances of their parameters.

The problem's objective function (13) takes the form

$$J\left[\mathbf{x}(k), \mathbf{y}(k), \mathbf{z}\right] = J_v\left[\mathbf{x}(k), \mathbf{y}(k)\right] + w_p J_p(\mathbf{z}) \tag{22}$$

where w_p a weighting parameter of the total penalty term, which depends on the problem size and properties; a value of 5.0 is used here.

Optimization problem (13)–(15), (22) is different from the one solved in (Poole and Kotsialos, 2016) in terms of the objective function used, which is based on a measurement vector which includes flows in addition to the speeds of (18). As a result, the weights used in the objective function (22) are also different.

4. Optimisation Algorithms Used for the Calibration Problem

4.1. PSO Algorithms

PSO (Eberhart and Kennedy, 1995; Kennedy and Eberhart, 1995) algorithms employ the notion of particles for searching the Γ dimensional solution space $C \subset \mathbb{R}^{\Gamma}$ having knowledge of the best previous solutions found by themselves and by other particles in their neighbourhood. This information is used to update a velocity (not to be confused with the vehicular mean speed) vector governing each particle's new position resulting to a flock converging towards the current best solution and evaluating the objective function at points along its flight path. An inertia weight (Shi and Eberhart, 1998) allows for the particles' velocity to have a momentum resulting to overshooting over the current optimum and explore more of the solution space.

PSO algorithms use different topologies for determining a particle's neighbourhood. Local-PSO (LPSO), also known as lbest PSO (Engelbrecht, 2013), (Kennedy and Mendes, 2002) uses a ring structure where each particle has two neighbours. There is a large body of literature concerned with variations of the basic search method. Seven different variants were used and their convergence properties are reported in (Poole and Kotsialos, 2016). Based on this work, LPSO (Kennedy and Mendes, 2002), Adaptive PSO (APSO) (Zhan et al., 2009) and High Exploration PSO (HEPSO) (Mahmoodabadi et al., 2014) have been selected for discussion along with RPROP. These three algorithms converged to the best model parameter sets; for further details see (Poole and Kotsialos, 2016).

The overall system architecture for EA based calibration is depicted in Figure 2. A simple interface between the search code and METANET allows to automatically set up all the necessary input files for METANET to run using any vector $\mathbf{z}$ given by (17). The objective function value (22) is calculated based on the simulation's output files. Since it is used as a black box the discretisation scheme followed does not depend explicitly on the sensors'

location. Instead, it is the sensors that are mapped to motorway segments after discretisation.

[Figure 2 about here.]

4.2. RPROP with ADOL-C

Problem (13)–(15) is a nonlinear constrained optimisation problem with equality and simple bound constraints. The equality constraints are given by the state equation (14) and simple bound constrains given by (15). The model's state equation, can be embedded iteratively directly into the objective function J and allowing to consider its dependence only on $\mathbf{z}$. In other words,

$$\begin{aligned} &J\left[\mathbf{x}(k), \mathbf{y}(k), \mathbf{z}\right] = \\ &J\left\{\mathbf{z}, \mathbf{y}(k), \mathbf{x}(k) : \mathbf{x}(k+1) = \mathbf{f}\left[\mathbf{x}(k), \mathbf{d}(k), \mathbf{z}\right], \mathbf{x}(0) = \mathbf{x}_0, k = 0, \ldots, K-1\right\} = \\ &J(\mathbf{z}) = J_v(\mathbf{z}) + w_p J_p(\mathbf{z}) \left(\text{from } (22)\right). \end{aligned} \tag{23}$$

where the dependence on $\mathbf{y}(k)$ has been dropped since these are known measurements.

The optimisation problem (13)–(15) can be expressed in view of (23) as

$$\min_{\mathbf{z}} J(\mathbf{z}) \tag{24}$$

subject to

$$\mathbf{z}_{\min} \leq \mathbf{z} \leq \mathbf{z}_{\max} \tag{25}$$

which is a simply bounded nonlinear optimisation problem. From (23)

$$\frac{\partial J}{\partial \mathbf{z}} = \frac{\partial J_v(\mathbf{z})}{\partial \mathbf{z}} + \frac{\partial J_p(\mathbf{z})}{\partial \mathbf{z}}. \tag{26}$$

$\partial J_p(\mathbf{z})/\partial \mathbf{z}$ can be calculated analytically from (21) since it consists of quadratic penalty terms and therefore

$$\frac{\partial J_p(\mathbf{z})}{\partial z_\gamma} = 2 \sum_{\ell=1, \ell \neq \mathcal{Z}_\gamma}^{\widehat{N}} w_{v,\rho,\alpha} \left(z_\gamma - z_\ell\right), \ \gamma = 1, \ldots, \Gamma \tag{27}$$

where $\mathcal{Z}_\gamma$ is the fundamental diagram index decision variable z_γ refers to and $w_{v,\rho,\alpha}$ is given from

$$w_{v,\rho,\alpha} = \begin{cases} w_v & \text{if } z_\gamma \text{ corresponds to a free speed} \\ w_\rho & \text{if } z_\gamma \text{ corresponds to a critical density} \\ w_\alpha & \text{if } z_\gamma \text{ corresponds to an exponent} \\ 0 & \text{otherwise.} \end{cases} \tag{28}$$

From the chain rule

$$\frac{\partial J_v(\mathbf{z})}{\partial \mathbf{z}} = \frac{\partial \mathbf{x}(\mathbf{z})}{\partial \mathbf{z}}^T \frac{\partial J(\mathbf{z})}{\partial \mathbf{x}(\mathbf{z})}. \tag{29}$$

In view of (11) $\partial J(\mathbf{z})/\partial \mathbf{x}(\mathbf{z})$ has the form

$$\frac{\partial J_v(\mathbf{z})}{\partial \mathbf{x}(\mathbf{z})} = \left[\frac{\partial J_v(\mathbf{z})}{\partial \mathbf{x}_1(k)}^T \cdots \frac{\partial J_v(\mathbf{z})}{\partial \mathbf{x}_{M_1}(k)}^T \right]^T, \; k = 1, \ldots, K \tag{30}$$

where

$$\begin{aligned} \frac{\partial J_v(\mathbf{z})}{\partial \mathbf{x}_m(k)}^T &= \left[\frac{\partial J_v(\mathbf{z})}{\partial \rho_{m,1}(k)} \frac{\partial J_v(\mathbf{z})}{\partial v_{m,1}(k)} \cdots \frac{\partial J_v(\mathbf{z})}{\partial \rho_{m,N_m}(k)} \frac{\partial J_v(\mathbf{z})}{\partial v_{m,N_m}(k)} \right]^T \\ & \quad m = 1, \ldots, M_1 \end{aligned} \tag{31}$$

Because of the quadratic nature of the error terms (19) and the fact that J_v in (20) does not explicitly depend on the densities

$$\frac{\partial J_v(\mathbf{z})}{\partial \rho_{m,i}(k)} = 0 \tag{32}$$

$$\begin{aligned} \frac{\partial J_v(\mathbf{z})}{\partial v_{m,i}(k)} &= \frac{2}{K M_5} \left[v_{m,i}(k) - y_{j,v}(k) \right] I_{m,i} \\ & \quad \forall\, m = 1, \ldots M_1,\; i = 1, \ldots, N_m,\; k = 1, \ldots, K \end{aligned} \tag{33}$$

with $I_{m,i}$ a binary indicator function showing if there is a measurement for segment (m, i) used in the error calculation and j is the corresponding measurement station in (18).

Equations (30)–(33) allow the analytical calculation of one of the right hand side terms of eqn. (29); in order to complete this calculation and determine its left hand side, the model's Jacobian matrix $\partial \mathbf{x}/\partial \mathbf{z}$ needs to be calculated. The matrix's structure is

$$\frac{\partial \mathbf{x}(\mathbf{z})}{\partial \mathbf{z}} = \begin{bmatrix} \frac{\partial \mathbf{x}(1)}{\partial z_1}^T & \cdots & \frac{\partial \mathbf{x}(1)}{\partial z_\Gamma}^T \\ \cdots & \cdots & \cdots \\ \frac{\partial \mathbf{x}(K)}{\partial z_1}^T & \cdots & \frac{\partial \mathbf{x}(K)}{\partial z_\Gamma}^T \end{bmatrix} \tag{34}$$

where

$$\frac{\partial \mathbf{x}(k)}{\partial z_\gamma}^T = \left[\frac{\partial \rho_{1,1}(k)}{\partial z_\gamma} \frac{\partial v_{1,1}(k)}{\partial z_\gamma} \cdots \frac{\partial \rho_{M_1,N_{M_1}}(k)}{\partial z_\gamma} \frac{\partial v_{M_1,N_{M_1}}(k)}{\partial z_\gamma} \right]^T \tag{35}$$

and because of (32) only the $\partial v_{m,i}(k)/\partial z_\gamma$ for every segment i of link m at time instant k with respect to every model parameter z_γ need to be calculated. This quantity is calculated by the ADOL-C AD library for every simulation time step. The whole Jacobian is calculated in a single simulation run based on the information encoded within METANET's source code. Hence, in order to obtain $\partial J(\mathbf{z})/\partial \mathbf{z}$ in (26), $\partial J_p/\partial \mathbf{z}$ and $\partial J_v/\partial \mathbf{x}$ are calculated analytically from (27) and (32)-(33), respectively, and $\partial \mathbf{x}/\partial \mathbf{z}$ is calculated by ADOL-C during a simulation run with METANET configured with $\mathbf{z}$.

It is this gradient calculation that RPROP utilises. RPROP has proved to be a fast and reliable search heuristic for converging to local minima for unconstrained, simply bounded, smooth and non-smooth problems, (Kotsialos, 2013), (Kotsialos, 2014) and for optimal control problems related to road traffic (Kotsialos and Papageorgiou, 2004) and production networks (Maropoulos et al., 2006). Since the optimisation problem (24), (25) is simply bounded, the projection operator is used on the gradient vector and decision variables' updates, see (Kotsialos, 2013).

Because RPROP does not posses the descent property it can perform search space exploration if allowed. Nevertheless, it needs to be paired by a globalisation technique in order to accelerate convergence and improve search space exploration. A simple multistart initialisation scheme where a number of individual instances of the same optimisation problem with initial points sampled from a Latin hypercube is sufficient.

A more complicated system architecture is necessary when coupling METANET with ADOL-C and RPROP, Figure 3. The RPROP application is the parent process invoking at each optimisation iteration the METANET executable. METANET is the child process and its role is to perform a single simulation run with the set of parameters sent by the parent and return back the Jacobian $\partial \mathbf{x}/\partial \mathbf{z}$. The two processes communicate using standard pipes commonly used in unix-like operating systems (linux in our case), writing the matrix in a shared memory area. The matrix $\partial \mathbf{x}/\partial \mathbf{z}$ is stored in memory shared by the child (METANET joined with ADOL-C) until the end of the simulation, i.e. until $k = K$. At this point, the whole $\partial \mathbf{x}/\partial \mathbf{z}$ is accessible by RPROP (the parent process) and the matrix multiplication (29) takes place. This way, bottleneck delays from the interprocess communication are avoided. This solution is depicted in Figure 3, where the Jacobian is directly accessible by the parent as it is stored in the shared memory after the simulation run.

[Figure 3 about here.]

Since a synchronized multistart version of RPROP is used, the parent process creates at each iteration the same number of child processes as the number of the different starting points sequentially. Once all the child processes deliver the required information the optimisation loop iteration index of the parent process is allowed to increase.

4.3. Algorithm Parameters

APSO, LPSO, HEPSO and RPROP are initialised using Latin hypercubes. Each decision variable is assumed to have a uniform distribution within its range, as defined in Table 1. For APSO, LPSO and HEPSO those limits are handled by moving solutions that are outside the domain, back to the boundary. The velocity component for dimensions that are adjusted this way is multiplied by -0.5 preventing solutions from attempting to leave the space at the next iteration. PSO algorithms have a population size set equal to 30. Other parameters are those given by the papers they were proposed in. The probabilities for the artificial bee colony and GA operators used by HEPSO are the same as those suggested by Mahmoodabadi et al. (2014). For LPSO the best results were obtained by using the parameter values suggested by Zambrano-Bigiarini et al. (2013).

RPROP convergence is heavily affected by the restart period. Restart is a typical feature of iterative gradient based algorithms whereby periodically a step along a different search direction, usually the steepest descent, is taken rather than the one selected by the algorithm. The restart process for RPROP is described in (Kotsialos, 2014), but here it is not periodic any more.

A short restart period allows the algorithm to rapidly try to explore new areas increasing this way the probability of finding a global minimum. However, time is required for the algorithm to fully exploit each basin of attraction, something that may be hindered by frequent restarts. It is not possible to know beforehand if a restart is going to be successful or not ending in the basin of attraction of a better local minimum. Instead of using a fixed restart period that could be too small or too large to be effective, a value was used that followed a chaotic sinusoidal mapping as suggested by Gandomi et al. (2013). The restart period randomly fluctuates then between its upper bound which was set at 200 and its minimum at 10 iterations. Similar to the swarm size of 30 used for the PSO algorithms, RPROP starts from 30 initial points which are updated synchronously.

5. Site Description and Data Availability

The test site is the Northbound M1 motorway as it enters Sheffield. It extends over 21.9 km and the METANET model consists of 20 links, Figure 4. Typically, recurrent congestion has the form of a shock wave originating at the centre. Usually it occurs at the end of the link L6.

[Figure 4 about here.]

It can be seen from Figure 4(b) that the entrance of M18 is modelled as two independent origins separated by link L6a. This reflects the junction's design where the on-ramp splits into two different merging lanes. The leftmost one leads the merging point 800 meter downstream the rightmost, hence link L6a.

For this site, MIDAS data were used from Monday the 1^{st}, 8^{th} and 15^{th} of June 2009. The only criterion used for selecting these datasets was that they should cover free flow, critical and congested conditions in order for the full spectrum of traffic dynamics to be represented. There was not any preliminary pre-selection phase or testing. Data from the same day of the week, a Monday, and the same time of day, 6:00 to 9:30 am, were extracted from the database. The data are quite similar because they represent the same time of the same day, but our study clearly shows that not all of them are suitable for use in a calibration problem. Differences in the boundary conditions are sufficient to render one them as unsuitable due to spillback. The MIDAS database provides large amounts of data reflecting the traffic conditions throughout the year. This provides the possibility of calibrating traffic flow models for different days and times of day. More detailed data oriented investigations may be organised based on the methodology provided here. However, this paper focuses on the details of the calibration and verification methods and provides a critical discussion of the results in terms of traffic quantities of interest. Emphasis is on describing the coupling of RPROP, METANET and ADOLC and the coupling of METANET with Evolutionary Algorithms, rather than the details of a possible data selection and model calibration campaigns under different sets of data varying time of day, day of week, environmental conditions and time of year.

The MIDAS data are collected from loop detectors installed on the motorways and the on-/off-ramps. MIDAS is a system owned by Highways England, which collects and archives on daily basis minute by minute flow, speed, and occupancy measurements per lane from highways in England.

It is well known that $v_{m,i}$ in eqn. (5) is the space mean speed, which for a small area centred around a loop detector is estimated by the harmonic mean of individual vehicle speeds passing over the detector. A method for estimating the space mean speed based on the lane time mean speed is described by Han et al. (2010) in an effort to improve travel time estimation accuracy. Here, a simpler approach is followed making the assumption that the traffic conditions are homogeneous along a lane, i.e. vehicles along a lane have the same speed. In this case the space and time mean speeds are identical for a lane flow stream.

Let k' denote the minute during which $N_{j,p}(k')$ vehicle counts are recorded yielding a time mean speed $\widehat{v}_{j,p}(k')$ at lane p of location j. Also, let $\widehat{v}_{j,p,a}(k')$ be the individual vehicle speeds whose arithmetic mean gives $\widehat{v}_{j,p}(k')$, i.e.

$$\widehat{v}_{j,p}(k') = \frac{1}{N_{j,p}(k')} \sum_{a=1}^{N_{j,p}(k')} \widehat{v}_{j,p,a}(k'). \tag{36}$$

Because of the assumption of equality of the time with the space mean speed at a lane, the measured speed can be expressed as the harmonic mean of individual speeds, i.e.

$$\widehat{v}_{j,p}(k') = \frac{N_{j,p}(k')}{\sum_{a=1}^{N_{j,p}(k')} \frac{1}{\widehat{v}_{j,p,a}(k')}} \Rightarrow \sum_{a=1}^{N_{j,p}(k')} \frac{1}{\widehat{v}_{j,p,a}(k')} = \frac{N_{j,p}(k')}{\widehat{v}_{j,p}(k')}. \tag{37}$$

The space mean speed of the road segment of link m which has λ_m lanes is estimated as the harmonic mean of all vehicles in it, i.e.

$$\begin{aligned} y_{j,v}(k') &= \left[\frac{1}{\sum_{p=1}^{\lambda_m} N_{j,p}(k')} \sum_{p=1}^{\lambda_m} \sum_{a=1}^{N_{j,p}(k')} \frac{1}{\widehat{v}_{j,p,a}(k')} \right]^{-1} \\ &= \frac{\sum_{p=1}^{\lambda_m} N_{j,p}(k')}{\sum_{p=1}^{\lambda_m} \sum_{a=1}^{N_{j,p}(k')} [\widehat{v}_{j,p,a}(k')]^{-1}} \text{ (and from (37))} \\ &= \left[\sum_{p=1}^{\lambda_m} \frac{N_{j,p}(k')}{\widehat{v}_{j,p}(k')} \right]^{-1} \sum_{p=1}^{\lambda_m} N_{j,p}(k'). \end{aligned} \tag{38}$$

Equation (38) accounts for the lateral speed variance in a road segment assuming no longitudinal variance in the estimation of the space mean speed.

This estimate is always smaller than the arithmetic of the measured lane speeds (36) with the difference increasing in congested traffic conditions. No other transformations on the data like those by Treiber and Kesting (2012) are used.

The site was modelled following METANET's nomenclature and the necessary files, as specified in (METANET, 2008), were developed. The information provided to the simulator is both static and dynamic. Static information is about the simulation mode (no control applied, with or without incidents, non-destination oriented and measurements' input pattern), which do not change during the optimisation iterations irrespective of the $\mathbf{z}$'s value and remain the same for repeated calls to the METANET executable. The network topology is static as well, but is encoded in a file together with the parameters $\mathbf{z}$. As a result when the objective function, and corresponding gradient, are evaluated for a particular $\mathbf{z}$, the network description file needs to be created on the fly.

Dynamic information comes in the form of trajectories of measurements over time at boundaries and at locations inside the site where data used for comparison exist. These data provide the model inputs, i.e. the initial state vector of eqn. (11) $\mathbf{x}(0)$, $\mathbf{d}$ as defined in eqn. (12) and the measurements' vector $\mathbf{y}$ in (18).

The demands at the origins for the three different days are shown in Figure 5 (a). METANET can accept speeds at origins but they are not necessary for the simulation to run. Still, they may improve model accuracy. With the exception of the main motorway entrance O1 at the upstream main site boundary and the leftmost lane of the M18 on-ramp O32-1, the speed is not given for on-ramps. Preliminary work showed improved convergence in the presence of speeds for those two locations. O1 is essentially the upstream motorway, hence the speed there is necessary as it influences the system dynamics; O32-1 is also a motorway lane where vehicles accelerate more than in the typical urban road. The speed trajectories are shown in Figure 5(b). Both the demand and the speed trajectories are very similar for the three days, reflecting the fact that they were taken from the Monday of three consecutive weeks of the same month.

[Figure 5 about here.]

Figure 6 shows the density trajectories at the network's destinations. There is no congestion at the end of the site at destination D1, hence there is

no congestion coming from downstream. The recurrent congestion occurring inside the network is endogenous. It is this kind of congestion a traffic flow model needs to be able to replicate and predict. Destinations D31, D32 and D34 are practically free flowing, with very low congestion levels. The road network just after those destinations has enough capacity for accommodating the outflows. This is not true, however, for destination D33, where an increase in density can be observed during the second half of the time horizon. The surface streets after D33 cannot accommodate the flow leaving the system and there is a density built up filling up the off-ramp lanes. This is a problematic condition because spillbacks are not explicitly modelled. To accommodate this situation, motorway link, L33 in Figure 4, was introduced.

[Figure 6 about here.]

Finally, Figure 7 shows the turning rates at each of the off-ramps. Driver's routing behaviour remains very similar for the 1st and 15th, with only small differences for the 8th. D32 and D33 carry out significant proportions of the total flow served by the network.

[Figure 7 about here.]

6. Model Calibration

As mentioned before, three data sets were selected for calibrating the model, from July 1st, 8th and 15th, 2009. The same METANET model was calibrated using APSO, LPSO, HEPSO (we refer to those as EA) and RPROP. Figures 8(a) and (b) depict the convergence profiles for the EA and RPROP, respectively, when solving problem (24)–(25) using the 15th's data. Subfigure (a) shows the objective function value over the number of iterations of particle number 1 in the swarm for each of the three EA. The corresponding algorithm's best of the whole swarm is depicted using lines. Particle number 1 achieves the best only for APSO after about 1,300 iterations, hence the concentration of points near the best line. For the other two algorithms, this specific particle does not achieve the optimum; the solid line (best particle) is produced by one of the untraced particles in the swarm. The erratic nature of EA's random search is clearly shown.

On the other hand, RPROP has a smoother, more targeted profile as can be seen in Figure 8(b). This reflects the nature of the gradient based

search performed. The spikes observed at each trajectory, are due to the restart. Because of the chaotic restart used, they occur at seemingly random iterations. RPROP does not require the large variance sampling EA use and is able to converge to the neighbourhood of the optimum faster.

[Figure 8 about here.]

LPSO and HEPSO required 75,030 function evaluations; for APSO this number is not static and approximately 76,500 were required for 2,500 iterations. An RPROP run with six points requires 15,012 function evaluations for the same number of iterations. An objective function evaluation performed within the framework of an EA algorithm, which does not require the evaluation of partial derivatives, takes 0.015 seconds. The same calculation in conjunction with the gradient vector evaluation based on ADOL-C and the matrix multiplication (29) requires 0.35 seconds. The ADOL-C routines were not optimised and speed up of the implementation is possible. It should be noted that contrary to gradient based line search and trust region methods, RPROP requires only one objective function value and one gradient vector evaluation per iteration. If such a method is used, the corresponding computation time increase should be compensated by increased speed of convergence.

Since the main aim of this paper is to demonstrate the coupling of METANET, ADOL-C and RPROP, rather than compare the performance of swarm and gradient based algorithms, each algorithm was run three times, each time with 30 particles (EA) and 30 start points (RPROP), to get some indicative comparison results. A more detailed investigation on the optimisation algorithmic performance will be reported for a much larger and more challenging network rather than the one used here.

Table 2 shows the objective function value (22) for each run of each day's data set and the corresponding square error averaged over time and number of detector stations, i.e. the expression given in (20). Since J_v is a square error, the resulting mean absolute error is in the order of 6 to 7 km/h.

[Table 2 about here.]

With the exception of HEPSO for the data of the 8th, the best result for J achieved by any of the swarm algorithms is also the best result with respect to the mean square error J_v. This is not true for RPROP as the

best J_v does not correspond to the best J. The penalty term for the optimal solution is larger in RPROP. This is to be expected, since RPROP has a larger number of degrees of freedom in the form of available decision variables representing a more detailed profile of model parameters. RPROP has 13 different fundamental diagrams at its disposal, which can be tuned, whereas the swarm algorithms are restrained to a maximum of 7 for the mainstream plus 2 separate ones for L32 and L33. In other words, in addition to the global parameters, which are the same for both types of algorithms, RPROP has 39 parameters (v_f, ρ_{cr} and α) for the available fundamental diagrams and PSO a maximum of 27. In fact, PSO algorithms converge to a solution where not all available fundamental diagrams are used. The difference in performance is quite small, since the mean absolute error remains in the area of 6 to 7 km/h.

The optimal solutions achieved by each algorithm for each of the data sets indicated by the bold font at Table 2 are given by Tables 3–6. The resulting spatial distribution of the capacity, free speed, critical density and α given by the optimal solutions obtained using the data of the 15th are depicted in Figures 9–11.

[Table 3 about here.]

[Table 4 about here.]

[Table 5 about here.]

[Table 6 about here.]

[Figure 9 about here.]

[Figure 10 about here.]

[Figure 11 about here.]

The results based on the data of the 8th are quite different from those obtained based on the other two days. What is observed at the table is the effect of using data that are unsuitable for model calibration. The reasons for this difference will be discussed in the next section.

It can be seen from Tables (4)–(6) and Figures 9–11 that APSO(1st), HEPSO(1st) and HEPSO(15th) converge to solutions that result to the same

capacity assignment pattern. Two different FD are used to model the mainstream; the first one starts from link L1 (beginning of the site) and extends to link L7. The second one starts from L8 extends up to L10 (the site's end). HEPSO(1st) and HEPSO(15th) split the mainstream into two sections with the upstream one to have high capacity and the downstream with lower. A slightly different pattern is followed by APSO(15th) where an additional FD is used for L10. LPSO(1st) also follows a two FD pattern but with different extension. The split takes place at L5 rather than L7.

RPROP(1st) and RPROP(15th) have a more complicated capacity pattern due to the larger number of available FD. The capacity pattern for section L7-L10 is the same and the two solutions differ on the mainstream part from L1–L5. These patterns reflect the fact that congestion is generated in the area of L6, hence the variance upstream of it.

A common feature of all solutions' capacity patterns is that the section that contains the last link L10 has always relatively smaller capacity. This is a very pronounced feature at the RPROP solutions as well as in APSO(15th). This tendency of the optimisation is not misplaced since the speed levels predicted by the model are close to those measured. This can be seen in Figure 12, where the measured and calibrated model speed trajectories based on RPROP(1st) and RPROP(15th) for the two segments of L10. It can be seen that the selection of the link's capacity is a trade-off between the two speed trajectories from the two segments, hence the small bias observed at the model speed for the second segment sending flows out of the system.

[Figure 12 about here.]

Another feature of the solutions are links L32 and L33, which have their own FD. They are auxiliary motorway links where dynamics are important for the overall model and they need to be described in more detail than the simple queueing of the origin links or the destinations' discharge. For RPROP(1st, 15th) L32's capacity is very similar to that of L6, into which it is feeding its traffic volume. Although this observation does not hold for the EA the RPROP solutions clearly support this.

No such connection can be identified for L33. This small link models a problematic interface with the surface street network, where congestion spilbacks occur. An explanation for the different capacities at the solutions of the 1st and 15th can be based on a closer examination of Figure 6 and the subdiagram showing the density at destination D33 where L33 leads.

During the period 8:55–9:10 am there is a pronounced difference between the destination density trajectories given as boundary conditions for D33. This density on the 15th remains high whereas on the 1st a sharp downwards peak can be seen. The hypothesis is that this difference on the boundary conditions is the cause for leading the capacity at the high level of 2,766 veh/km/lane for the 1st and at the level of 1,622 veh/km/lane for the 15th. Further evidence supporting it are the solutions delivered by the EA for L33.

Overall, all algorithms provide parameter sets that are able to reproduce the traffic dynamics with very good accuracy. Figure 13 provides the calibrated model, based on the optimal solutions found by each algorithm, versus speed measurements diagrams. Figure 14 depicts the distance-time diagrams of the calibrated METANET model of the 15th using the parameter sets resulting to the minimum J_v on Table 2 for each of the four optimisation algorithms. Empty spaces on them indicate areas where there are no data available.

[Figure 13 about here.]

[Figure 14 about here.]

An additional insight on how the mean speeds are related to the model parameters for which the calibration problem is solved, can be obtained by the information contained in the Jacobian matrix $\partial\mathbf{x}/\partial\mathbf{z}$. In effect this matrix provides the sensitivities of the segments' mean speed at every point in time with respect to all variables included in $\mathbf{z}$. These sensitivities can be displayed on distance-time diagrams similar to Figure 14. The result is an additional insight on systems dynamics and how sensitivities propagate inside the network.

Figure 15 shows the sensitivity of the network's speeds over the whole time horizon with respect to the FD parameters of links L1, L6 and L10 for the solution obtained by RPROP(15th). Sensitivity shockwaves can be seen depending on the links' locations. Forwards moving shockwaves can be observed for the sensitivity to L1's parameters, from the site's start towards its end. Backwards shockwaves can be seen for the sensitivities with respect to the L10 FD parameters propagating from the site's end towards the start. A more complicated pattern in the area where congestion forms can be seen on link's L6 diagram. Figure 16 depicts the speed sensitivities with respect to the global parameters. All sensitivities are evaluated for the

specific boundary conditions of the particular day at the solutions given by Tables 3–6.

[Figure 15 about here.]

[Figure 16 about here.]

This information can be used for systematic analysis of motorway features, such as bottlenecks over time and space. Control strategy design can benefit as well as infrastructure improvement projects. It is beyond the scope of this paper to present a detailed study of the model's sensitivity dynamics and how this information is to be exploited and is left as future work.

In order to judge the quality of solutions obtained and their relevance to real traffic, a verification process needs to take place. This entails the use of the optimal parameter sets on data that were not used for the corresponding calibration optimisation problem. The next section is concerned with model verification.

7. Model Verification

The discussion on model verification requires testing of the optimal parameter sets obtained from the solution of the calibration problems. In order to facilitate it, the optimal parameter sets obtained by *algorithm* based on data from *date* are denoted as $\mathbf{z}^*_{algorithm(date)}$. When *algorithm* is omitted we refer to the best $\mathbf{z}$ of the day.

Each of the optimal parameter sets given by Tables 3–6 was used for running a simulation with boundary conditions data (demands, densities and turning rates) from the other two. In each case J_v was calculated according to (20). Table 7 provides the values of J_v for the all $\mathbf{z}^*$, algorithms and dates.

[Table 7 about here.]

The diagonal elements in each algorithm block of the table are the minimum row values since they are the calibrated solutions to the specific date. The degradation of the model quality as demonstrated at the other two row entries is to be expected, since the parameters were not optimised for the corresponding set of data.

It can be seen from Table 7 that the optimal parameter vectors of the 15th are able to reproduce the congestion pattern of the 1st better than the

other way around. When $\mathbf{z}^*_{1st}$ is applied on the data of the 15th, J_v increases by a nearly constant factor of 2.8 times the calibration error of the 1st. When $\mathbf{z}^*_{15th}$ is applied on the data of the 1st, the error increases by a factor of about 1.6 for the EA and 2.6 for RPROP. Hence, it can be concluded that the data of the 15th provide more information about the underlying traffic dynamics and the optimisation algorithms produce more relevant sets of parameters The value of J_v in these cases ranges from 77 to 83 $(\text{km/h})^2$, i.e. from 8.8 to 9.1 km/h per measurement, which is a very small difference and is consistent to what is reported in the literature (Spiliopoulou et al., 2014), (Ngoduy and Maher, 2012).

The main source of verification error comes from underestimating the congestion's queue tail extension and duration. Figure 17 shows the model and corresponding speed measurements when $\mathbf{z}^*_{15th}$ is used for the data of the 1st. The speed dynamics are accurately represented for the site, with the exception of an area outlined by two detector stations that is about 700 meters long. The model predicts for this length of road a faster speed recovery than the one observed, by about 40 minutes. The reasons for this result are not clear, but in view of the fact that solutions based on the 1st do not generalise as well as those based on the 15th, it could be attributed to an exogenous or irregular event factor. This behaviour is consistent with verification results reported in the literature, (Spiliopoulou et al., 2014). However, the overall congestion dynamics are reproduced with sufficient accuracy as can be seen from the resulting distance-time diagram in Figure 18.

[Figure 17 about here.]

[Figure 18 about here.]

Another pronounced feature on Table 7 is the poor generalisation of the parameters obtained based on data from the 8th. Although the calibration error is at the same level as for the other dates, once the $\mathbf{z}^*_{8th}$ of any algorithm is applied to any other date, the error becomes very large. A similar degradation is observed when one of the $\mathbf{z}^*_{1st}$ or $\mathbf{z}^*_{15th}$ is applied on the data of the 8th, signalling a problematic situation on that particular day.

A closer examination of the data leads to the conclusion that there is a prolonged spilback of congestion from the surface are into the motorway from D33 for this date. Figure 19 depicts the mean speed trajectories of every lane of link L6 for the three days of data. A recurrent drop of speed

can be observed. The speed drop on the 8th for the first lane is much higher than in the other days but also it is higher compared with the other two lanes. This is a spilback of congestion from L33 and D33 during the short period of 07:40–07:54.

[Figure 19 about here.]

This effect is exogenous to the traffic dynamics of the system since it is caused by the traffic conditions of the surface streets. In order to compensate for it a small incident was introduced at L33 for the duration of the speed drop. L33's capacity was dropped to 875 veh/hour/lane, or 1,750 veh/hour for both lanes, during this period. The outcome of this intervention is shown on the last column of Table 7; the average square mean error is reduced for all parameter sets. Based on the results of Table 7, $\mathbf{z}^*_{RPROP(15th)}$ is the best set of parameters identified.

8. Conclusion and Future Work

This paper has presented a detailed study on macroscopic traffic flow model validation using a number of different optimisation algorithms. The focus has been on gradient based optimisation but results from evolutionary algorithms were presented as well. The underlying model used is the well-known METANET simulator, which has been combined with automatic differentiation software (ADOL-C) and numerical optimisation (RPROP) for developing a system of traffic flow model parameter estimation. The additional requirement of automatically selecting each fundamental diagram's location and extension is an explicit feature of the evolutionary optimisation algorithms but not of the gradient based. This constraint is implicitly considered in the optimisation problem formulation where variations of fundamental diagram parameters are penalised.

Data from three different days were used for calibration and verification. It has been shown that not all data given as input for parameter identification were suitable for this purpose. Their ability to guide optimisation algorithms to converge to solutions encapsulating the underlying traffic flow dynamics is not always present. In fact this study raises the question of how to qualify sets of data to be used for calibration. All three data sets used display a recurrent and relatively regular pattern of congestion. However, only one of them proved to be suitable for calibration. A good result from

the optimisation algorithm minimising the error is not a sufficient indicator of a valid model. The general rule of thumb for selecting data sets ensuring representative measurements of free, critical and congested conditions is not enough neither. Complex interactions may be overlooked resulting to non-representative parameters and therefore a severe model–reality mismatch. Sufficient criteria and conditions need to be determined in order to automate this qualification process, something which can be based on the notion of persistence of excitation.

The solution of the calibration problem using gradient based optimisation is one of this paper's original contributions. It has been demonstrated here that the calculation of the necessary partial derivatives is possible by using automatic differentiation software technology. The ADOL-C library employed has proven to be a highly flexible and robust piece of software that can be easily incorporated into the source code of a macroscopic traffic flow simulator. A by-product of the overall gradient calculation, is the calculation of the state's Jacobian matrix with respect to the model parameters. This yields additional information regarding the mean speeds' sensitivities with respect to the infrastructure-vehicle-driver parameters that can be exploited for improving control design and interventions to the traffic system. A more detailed investigation of how these sensitivities can be utilised in a rigorous and systematic manner is a future direction of research.

The fact that gradient information has become available opens the way for using well known and established optimisation methods. In this paper the RPROP algorithm as an optimisation search heuristic has been used. It has been shown that it is capable of solving this highly complicated and demanding problem. Its simplicity of implementation has allowed the integration of the three different source codes into a single system, i.e. METANET, ADOL-C and RPROP.

Results from swarm intelligence and RPROP have been presented here. A more detailed evaluation of algorithmic speed of convergence and solution quality will take place for a significantly larger and challenging network. Another line of research following this work is using other second order macroscopic traffic flow models that do not suffer from the isotropy assumption. Further work will also focus on improving the software implementation issues and RPROP's speed of convergence. Implementing integer programming methods for the problem formulation where a maximum number of used FD constraint is imposed is another important area of work. Finally, more detailed experiments need to be conducted in order to correlate the capacity, as

calculated by the calibration, and traffic composition with respect to different vehicle classes in it.

Acknowledgements

The authors would like to thank EPSRC for partially supporting this work and the Highways England for providing the necessary traffic data and related information.

References

Alessandri, A., Bolla, R., Grassia, A., Repetto, M., June 2006. Identification of freeway macroscopic models using information from mobile phones. In: American Control Conference. pp. 3801–3806.

Box, M. J., 1965. A new method of constrained optimization and a comparison with other method. The Computer Journal 8 (1), 42–52.

Cremer, M., Papageorgiou, M., 1981. Parameter identification for a traffic flow model. Automatica 17 (6), 837–843.

Daganzo, C., 1994. The Cell Transmission Model: A dynamic representation of highway traffic consistent with the hydrodynamic theory. Transportation Research Part B 28, 269–287.

Eberhart, R., Kennedy, J., 1995. A new optimizer using particle swarm theory. In: Proc. 6th Inter. Symp. on Micro-machine and Human Science. IEEE, pp. 39–43.

Engelbrecht, A., Sept 2013. Particle Swarm Optimization: Global Best or Local Best? In: Computational Intelligence and 11th Brazilian Congress on Computational Intelligence (BRICS-CCI CBIC), 2013 BRICS Congress on. pp. 124–135.

Fletcher, R., 2013. Practical methods of optimization. John Wiley & Sons.

Frejo, J. R. D., Camacho, E. F., Horowitz, R., 2012. A parameter identification algorithm for the METANET model with a limited number of loop detectors. In: Proc. 51st IEEE Conference on Decision and Control. pp. 6983–6988.

Gandomi, A. H., Yun, G. J., Yang, X.-S., Talatahari, S., 2013. Chaos-enhanced accelerated particle swarm optimization. Communications in Nonlinear Science and Numerical Simulation 18 (2), 327–340.

Han, J., Polak, J., Barria, J., Krishnan, R., 2010. On the estimation of space-mean-speed from inductive loop detector data. Transportation Planning and Technology 33, 91–104.

Helbing, D., Hennecke, A., Shvetsov, V., Treiber, M., 2002. Micro- and macro-simulation of freeway traffic. Mathematical and Computer Modelling 35 (5–6), 517–547.

Kennedy, J., Eberhart, R., 1995. Particle swarm optimization. In: Proc. IEEE Int. Conf. on Neural Networks. Vol. 4. IEEE, pp. 1942–1948.

Kennedy, J., Mendes, R., 2002. Population structure and particle swarm performance. In: Proc. of the World Congress on Computational Intelligence. Vol. 2. IEEE, pp. 1671–1676.

Kontorinaki, M., Spiliopoulou, A., Papamichail, I., Papageorgiou, M., Tyrinopoulos, Y., Chrysoulakis, J., 2015. Overview of nonlinear programming methods suitable for calibration of traffic flow models. Operational Research 15 (3), 327–336.

Kotsialos, A., 2013. Non-smooth optimization based on resilient backpropagation search for unconstrained and simply bounded problems. Optimization Methods and Software 28 (6), 1282–1301.

Kotsialos, A., 2014. Nonlinear optimisation using directional step lengths based on RPROP. Optimization Letters 8 (4), 1401–1415.

Kotsialos, A., Papageorgiou, M., 2004. Nonlinear optimal control applied to coordinated ramp metering. IEEE Transactions on Control Systems Technology 12 (6), 920–933.

Kotsialos, A., Papageorgiou, M., Diakaki, C., Pavlis, Y., Middelham, F., 2002. Traffic flow modeling of large-scale motorway networks using the macroscopic modeling tool METANET. IEEE Trans. Intell. Transp. Syst. 3 (4), 282–292.

Kotsialos, A., Pavlis, Y., Middelham, F., Diakaki, C., Vardaka, G., Papageorgiou, M., 1998. Modelling of the large scale motorway network around amsterdam. Preprints of the 8th IFAC Symposium on Large Scale Systems 2, 354–360.

Kotsialos, A., Poole, A., Oct 2013. Autonomic systems design for ITS applications. In: 2013 16th International IEEE Conference on Intelligent Transportation Systems. pp. 178–183.

Kotsialos, A., Poole, A., 2016. Autonomic Systems Design for ITS Applications Modelling and Route Guidance. In: Kotsialos, A., Müller, J., Schumann, R., McCluskey, L., Rana, O., Klügl, F. (Eds.), Autonomic Road Transport Support Systems. Birkhäuser, pp. 131–145.

Lighthill, M., Whitham, G., 1955. On kinematic waves II: a traffic flow theory on long crowded roads. Proc. Roy. Soc. London Series A 229, 317–345.

Luspay, T., Kulcsár, B., van Wingerden, J., Verhaegen, M., 2009. On the identification of lpv traffic flow model. In: Control Conference (ECC), 2009 European. IEEE, pp. 1752–1757.

Luspay, T., Kulcsár, B., van Wingerden, J., Verhaegen, M., Bokor, J., Jan 2011. Linear parameter varying identification of freeway traffic models. IEEE Transactions on Control Systems Technology 19 (1), 31–45.

Luspay, T., Kulcsár, B., Varga, I., Bokor, J., 2010. Parameter-dependent modeling of freeway traffic flow. Transportation Research Part C: Emerging Technologies 18 (4), 471–488.

Mahmoodabadi, M. J., Salahshoor Mottaghi, Z., Bagheri, A., 2014. HEPSO: High exploration particle swarm optimization. Information Sciences 273, 101–111.

Maropoulos, P., Kotsialos, A., Bramall, D., 2006. A theoretical framework for the integration of resource aware planning with logistics for the dynamic validation of aggregate plans within a production network. CIRP Annals-Manufacturing Technology 55 (1), 483–488.

Messmer, A., Papageorgiou, M., 1990. METANET: A macroscopic simulation program for motorway networks. Traffic Engineering and Control 31, 466–470; 549.

METANET, 2008. "METANET Documentation". Dynamic Systems and Simulation Laboratory, Technical University of Crete, Chania, Crete, Greece.

Munoz, L., Sun, X., Horowitz, R., Alvarez, L., 2006. A piecewise-linearized cell transmission model and parameter calibration methodology. In: Proc. of the 85th Transportation Research Board Annual Meeting. Washington D.C., USA, pp. 183–191.

Munoz, L., Sun, X., Sun, D., Gomes, G., Horowitz, R., 2004. Methodological calibration of the cell transmission model. In: Proc. of the 2004 American Control Conf. Boston, MA, USA, pp. 798–803.

Nelder, J., Mead, R., 1965. A simplex method for function minimization. The Computer Journal 7 (4), 308–313.

Ngoduy, D., Hoogendoorn, S., Van Zuylen, H., 2004. Comparison of numerical schemes for macroscopic traffic flow models. Transportation Research Record 1876 (1), 52–61.

Ngoduy, D., Maher, M., 2012. Calibration of second order traffic models using continuous cross entropy method. Transportation Research Part C 24, 102–121.

Nocedal, J., Wright, S., 2006. Numerical optimization. Springer Science & Business Media.

Papageorgiou, M., 1983. Applications of automatic control concepts to traffic flow modeling and control. Vol. 50 of Lecture Notes in Control and Information Sciences. Springer.

Papageorgiou, M., Blosseville, J.-M., Hadj-Salem, H., 1990. Modelling and real-time control of traffic flow on the southern part of Boulevard Peripherique in Paris: Part I: Modelling. Transportation Research Part A 24 (5), 345–359.

Payne, H. J., 1971. Models of freeway traffic and control. Proc. Simulation Council 28, 51–61.

Poole, A., Kotsialos, A., 2012. METANET model validation using a genetic algorithm. In: Proc. of the 13th IFAC Symp. on Control in Transportation Systems. pp. 7–12.

Poole, A., Kotsialos, A., 2016. Swarm intelligence algorithms for macroscopic traffic flow model validation with automatic assignment of fundamental diagrams. Applied Soft Computing 38, 134–150.

Richards, P. I., 1956. Shock waves on the highway. Operations Research 4, 42–51.

Riedmiller, M., Braun, H., 1993. A direct adaptive method for faster backpropagation learning: The rprop algorithm. In: Neural Networks, 1993., IEEE International Conference on. IEEE, pp. 586–591.

Shi, Y., Eberhart, R., 1998. A modified particle swarm optimizer. In: Proc. IEEE World Congress on Computational Intelligence. IEEE, pp. 69–73.

Spiliopoulou, A., Kontorinaki, M., Papageorgiou, M., Kopelias, P., 2014. Macroscopic traffic flow model validation at congested freeway off-ramp areas. Transportation Research Part C 41, 18–29.

Spiliopoulou, A., Papamichail, I., Papageorgiou, M., Tyrinopoulos, I., Chrysoulakis, J., 2015. Macroscopic traffic flow model calibration using different optimization algorithms. Transportation Research Procedia 6, 144–157.

Treiber, M., Kesting, A., 2012. Validation of traffic flow models with respect to the spatiotemporal evolution of congested traffic patterns. Transportation Research Part C 21 (1), 31–41.

Walther, A., Griewank, A., 2012. Getting started with ADOL-C. Combinatorial Scientific Computing, 181–202.

Whitham, G. B., 1974. Linear and nonlinear waves. John Wiley & Sons.

Zambrano-Bigiarini, M., Clerc, M., Rojas, R., 2013. Standard particle swarm optimisation 2011 at CEC-2013: A baseline for future PSO improvements. In: IEEE Congress on Evolutionary Computation. pp. 2337–2344.

Zhan, Z., Zhang, J., Li, Y., Chung, H., 2009. Adaptive particle swarm optimization. IEEE Transactions on Systems Man and Cybernetics B 39 (6), 1362–1381.

List of Figures

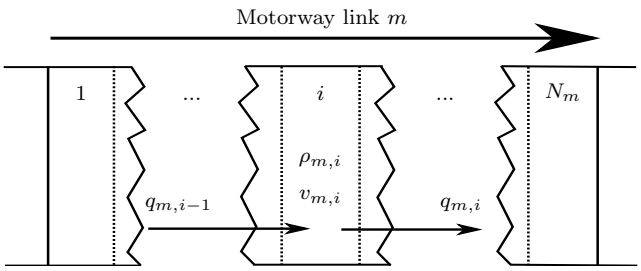

Figure 1: Link discretisation.

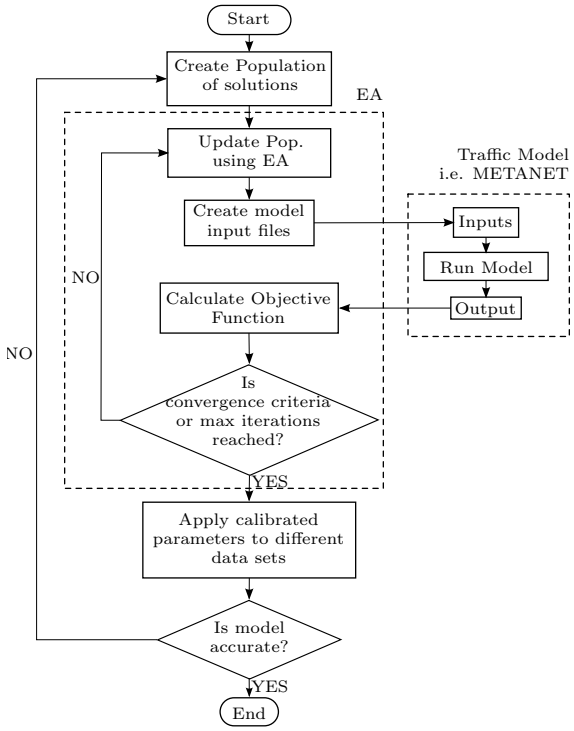

Figure 2: PSO based system architecture.

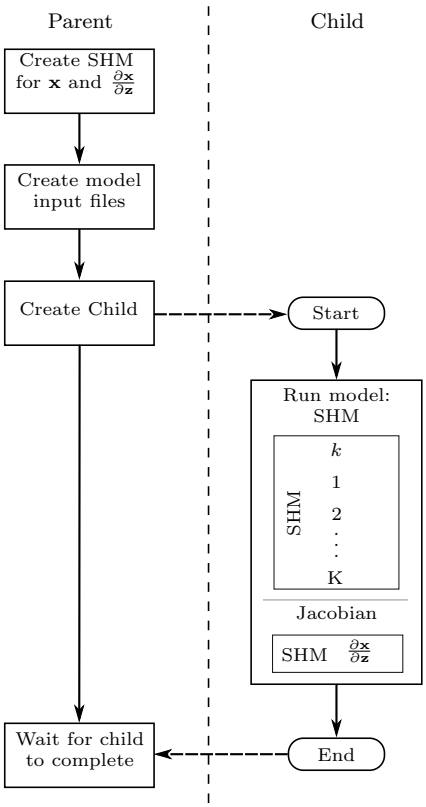

Figure 3: RPROP–METANET–ADOL-C system architecture (SHM stands for shared memory).

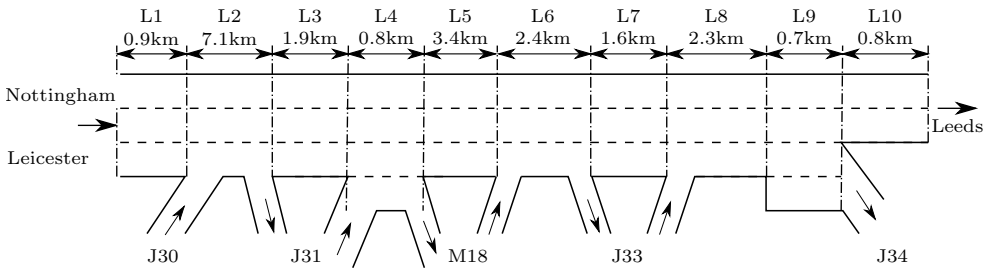

(a)

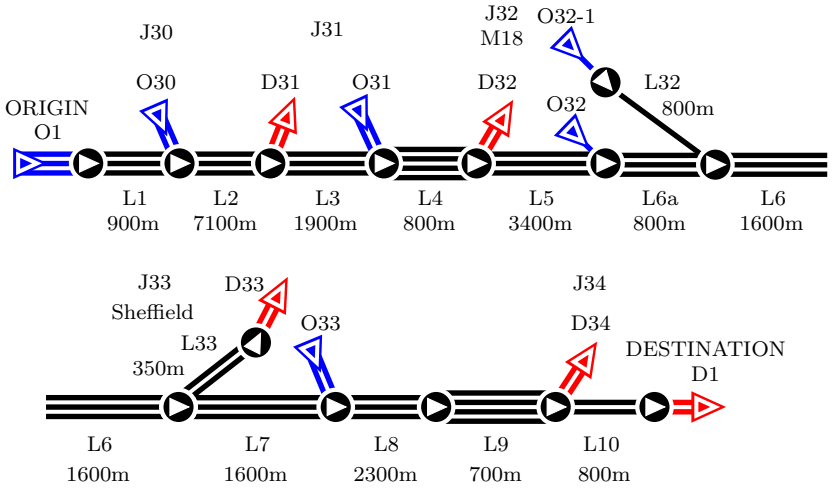

(b)

Figure 4: (a) Outline of Sheffield site. (b) METANET model. (not to scale)

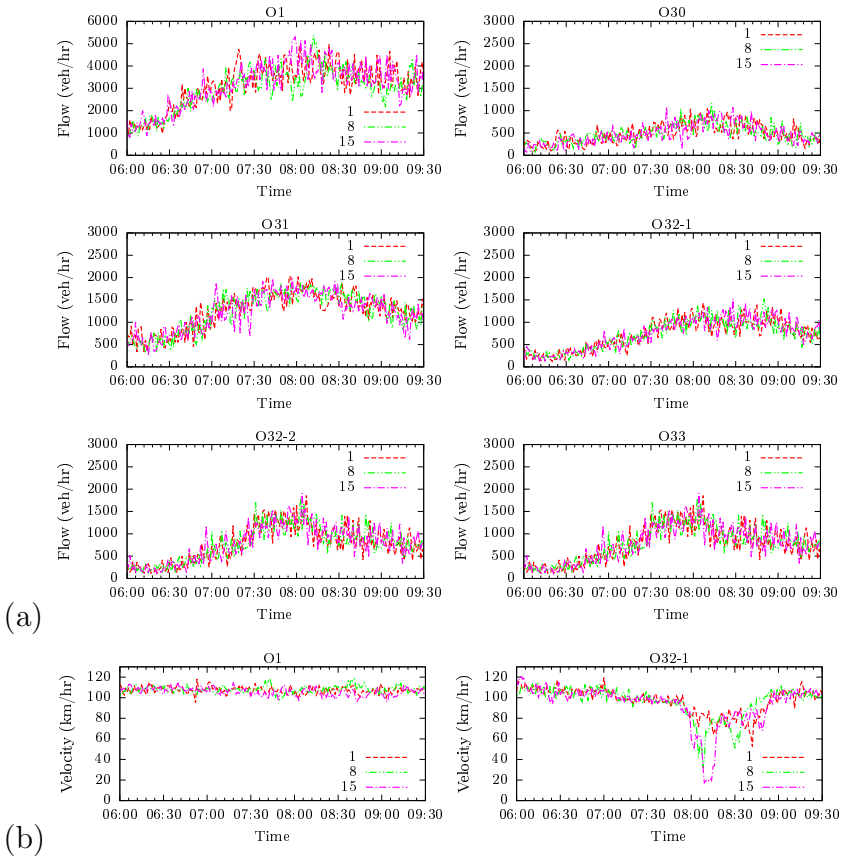

Figure 5: Measurements used as input at origin links for the three days. (a) Demand. (b) Mean speed.

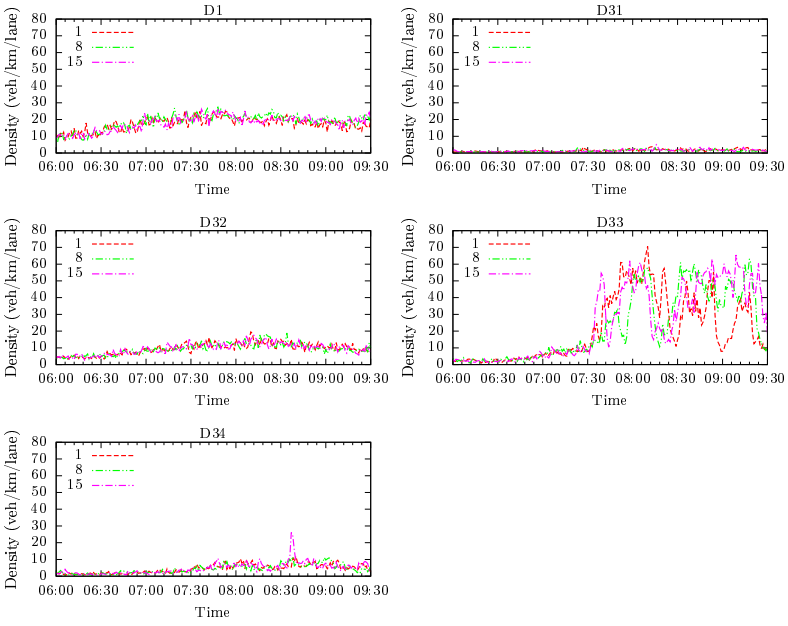

Figure 6: Density trajectories at the destinations for the three sets of data.

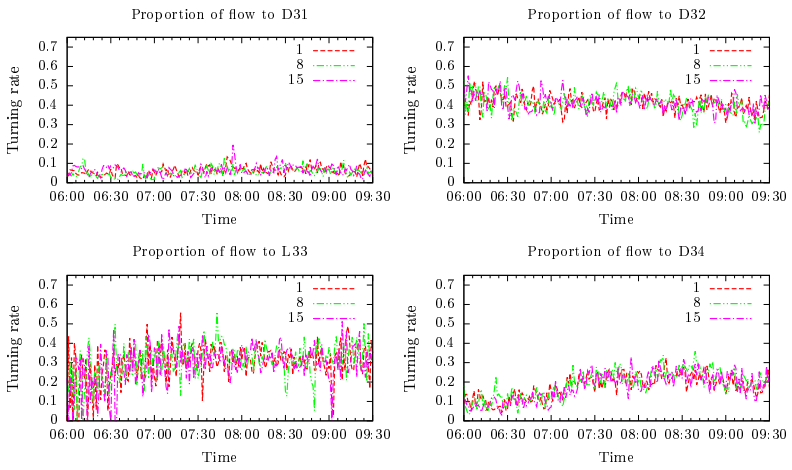

Figure 7: Turning rates trajectories for each off-ramp for the three sets of data.

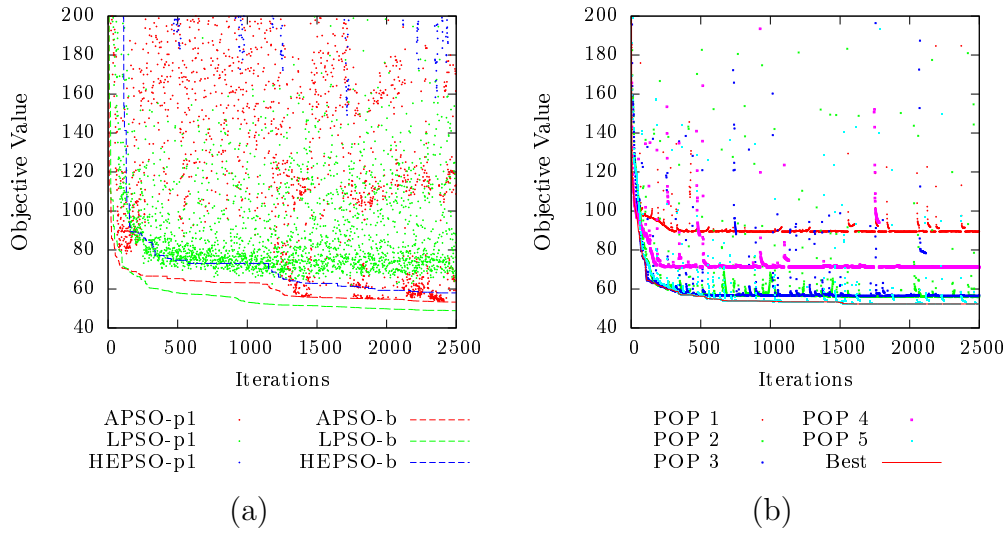

Figure 8: Convergence profiles for the data of the 15th. (a) APSO, APSO and HEPSO particle 1 of the swarm and best value (*algorithm*-b). (b) Multistart RPROP from five initial points and the current best. "Best" lines show the minimum value of the objective function found by the current iteration.

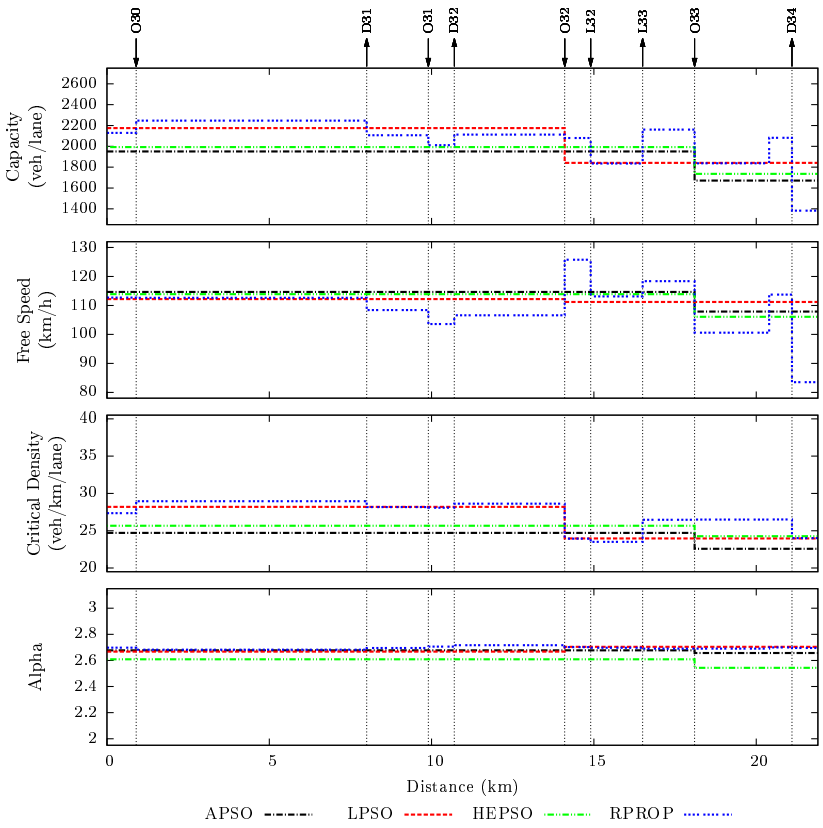

Figure 9: FD parameters' spatial distribution from the calibration optimal solutions found by the four optimisation algorithms using data of the 1st.

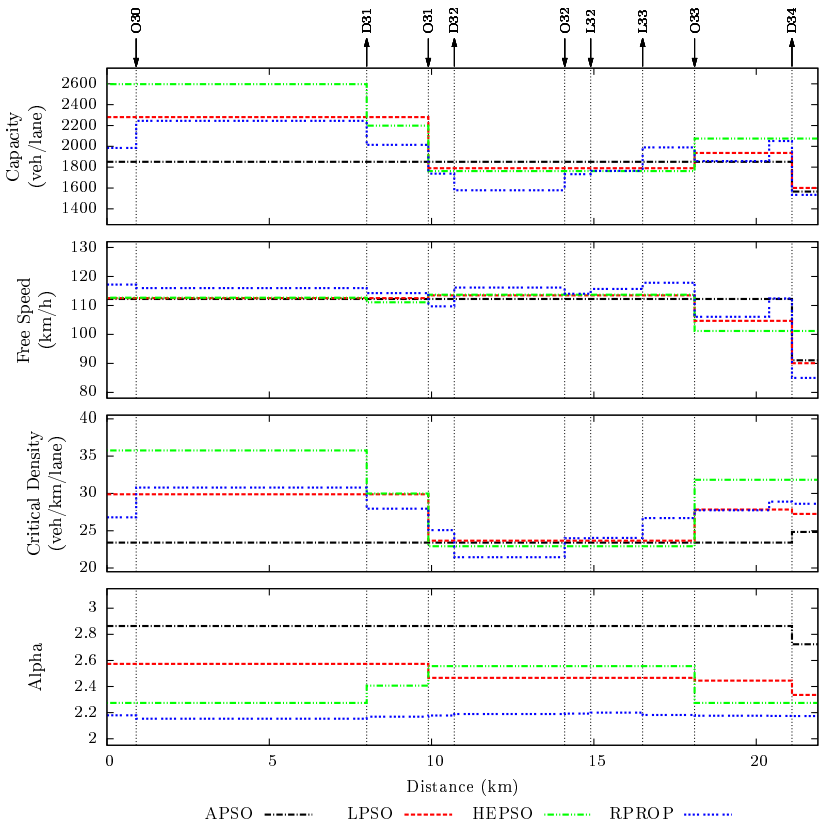

Figure 10: FD parameters' spatial distribution from the calibration optimal solutions found by the four optimisation algorithms using data of the 8th.

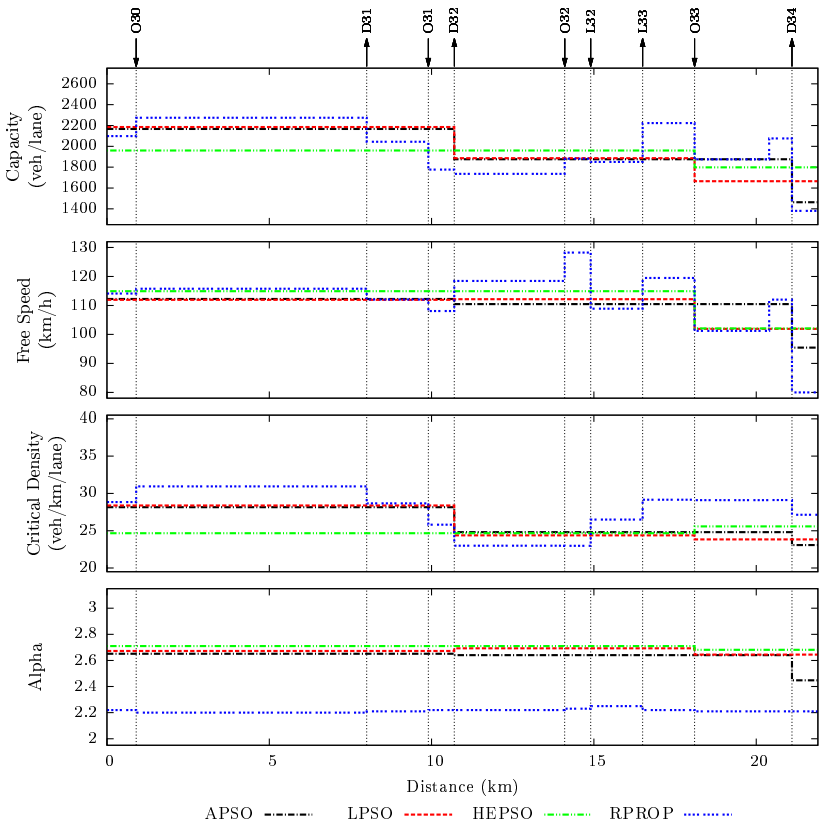

Figure 11: FD parameters' spatial distribution from the calibration optimal solutions found by the four optimisation algorithms using data of the 15th.

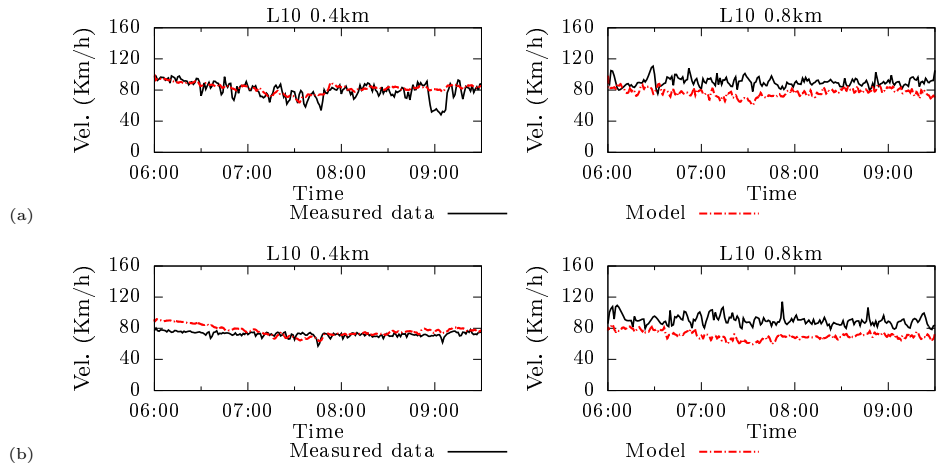

Figure 12: Measured and model speeds for the two segments of L10 calibrated using RPROP based on the data of (a) the 1st and (b) the 15th.

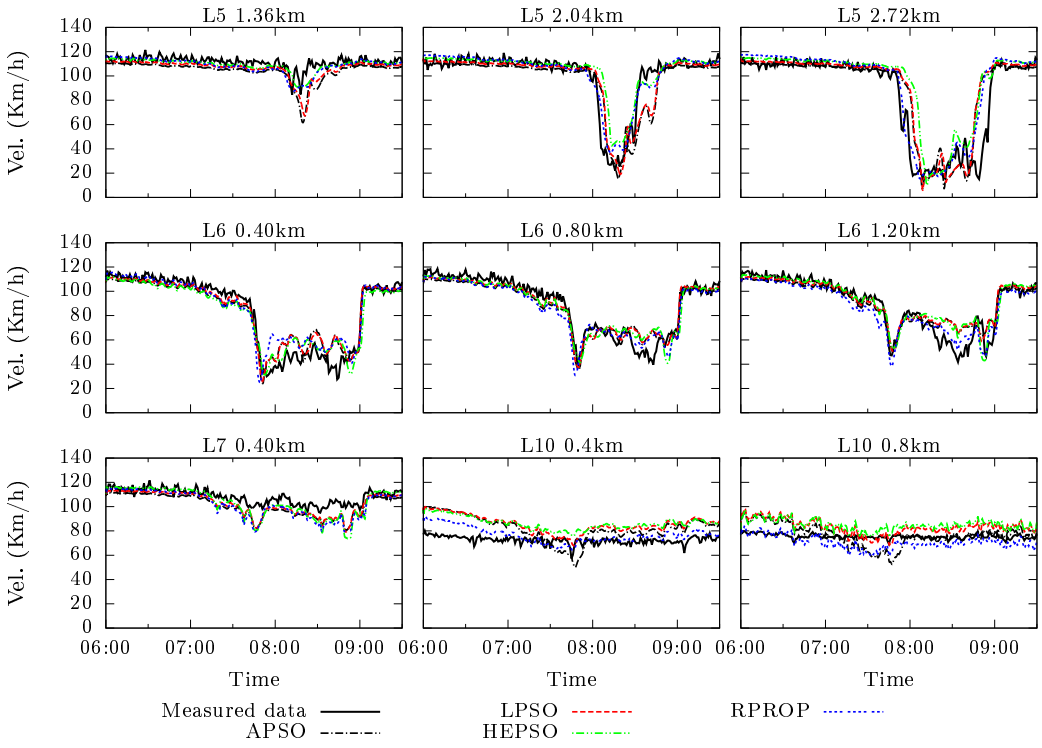

Figure 13: Calibrated model versus measured speeds for the data of the 15th.

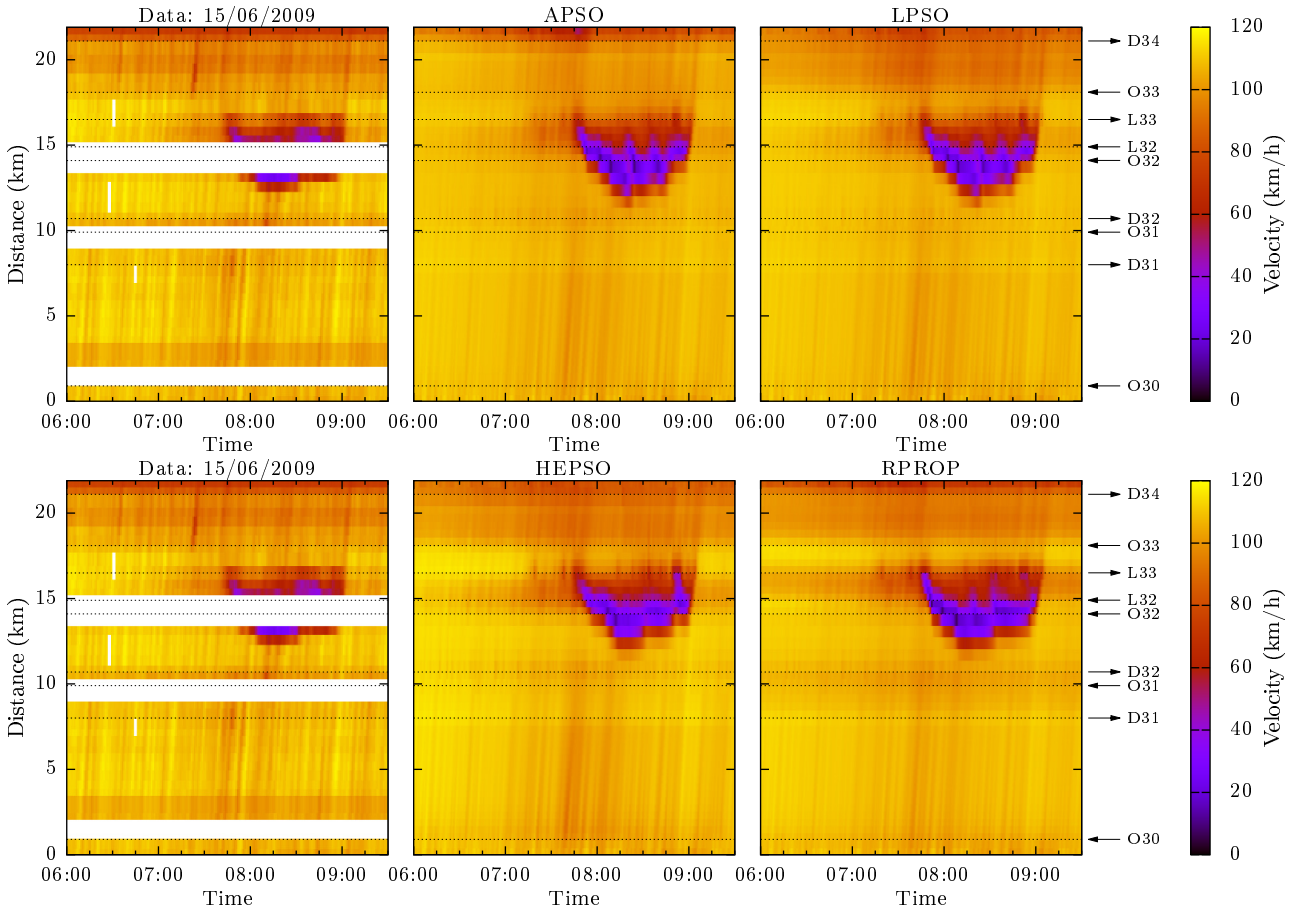

Figure 14: Distance-time diagram for calibration using the data of the 15th.

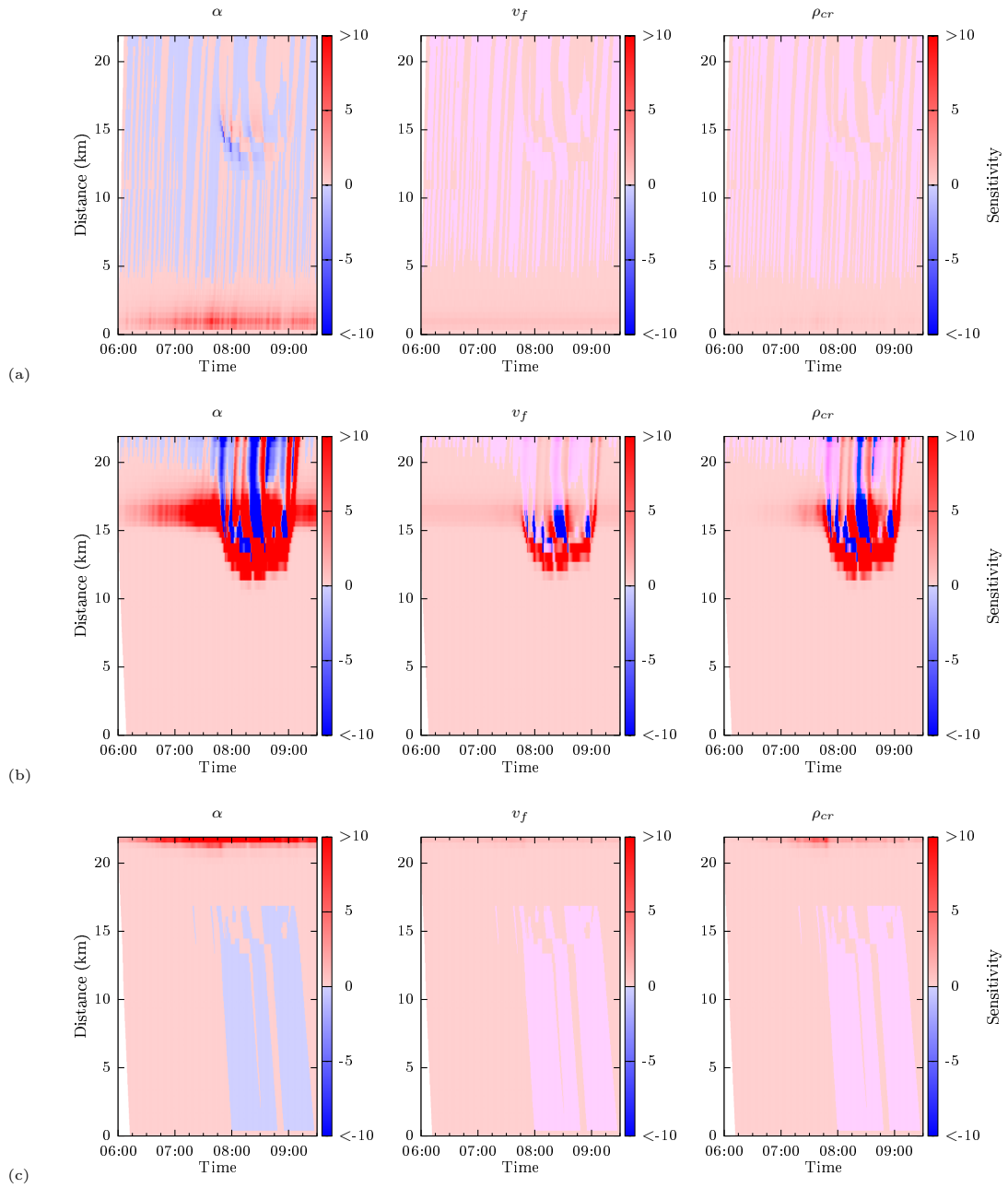

Figure 15: Network mean speed sensitivities to the FD parameters calculated by RPROP(15th) of links (a) L1 (b) L6 (c) L10.

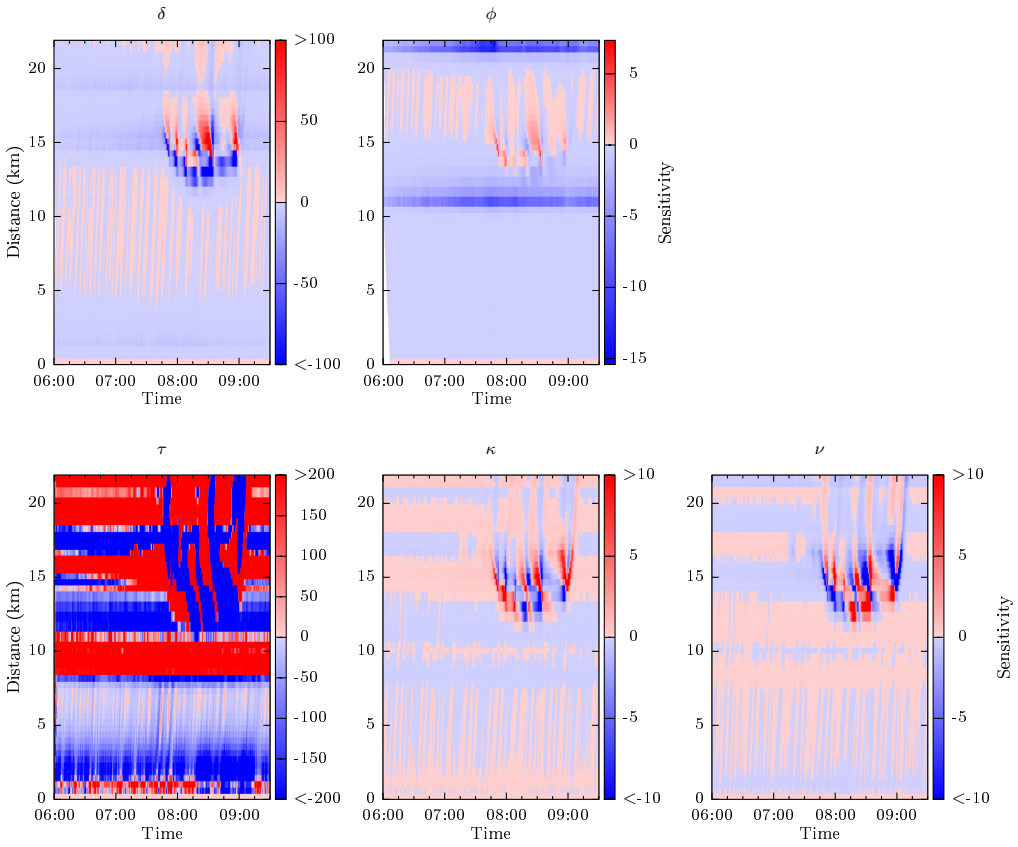

Figure 16: Network mean speed sensitivities to the global model parameters calculated by RPROP(15th).

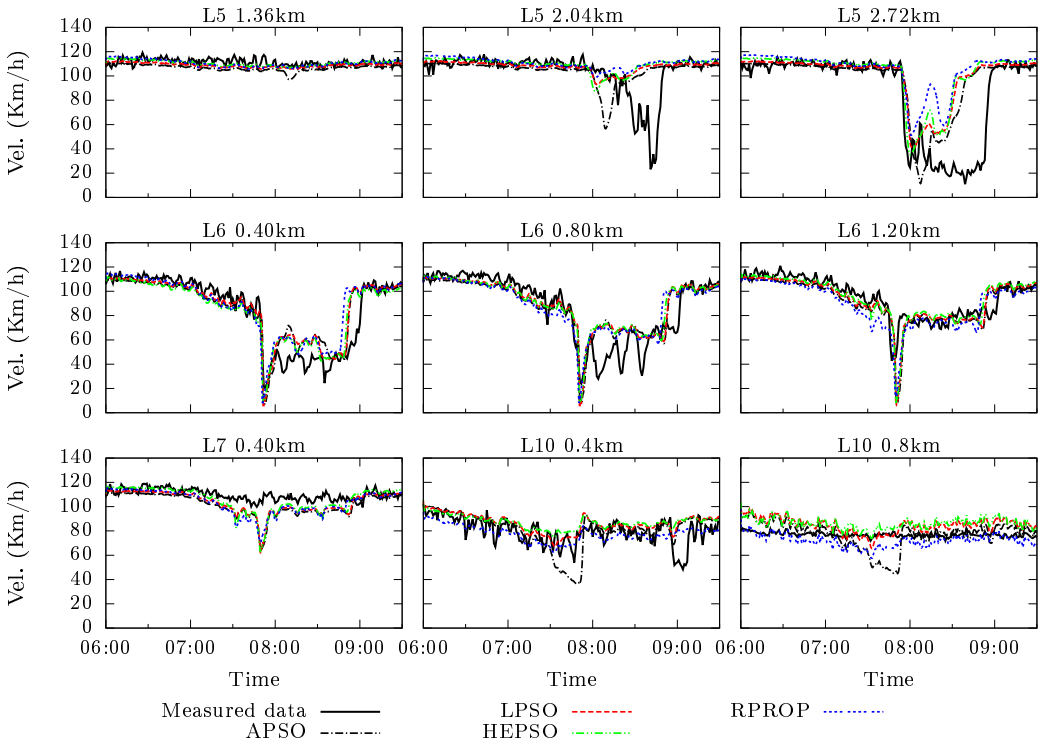

Figure 17: Model versus speed measurements when $\mathbf{z}^*_{15th}$ is used with the data of the 1st.

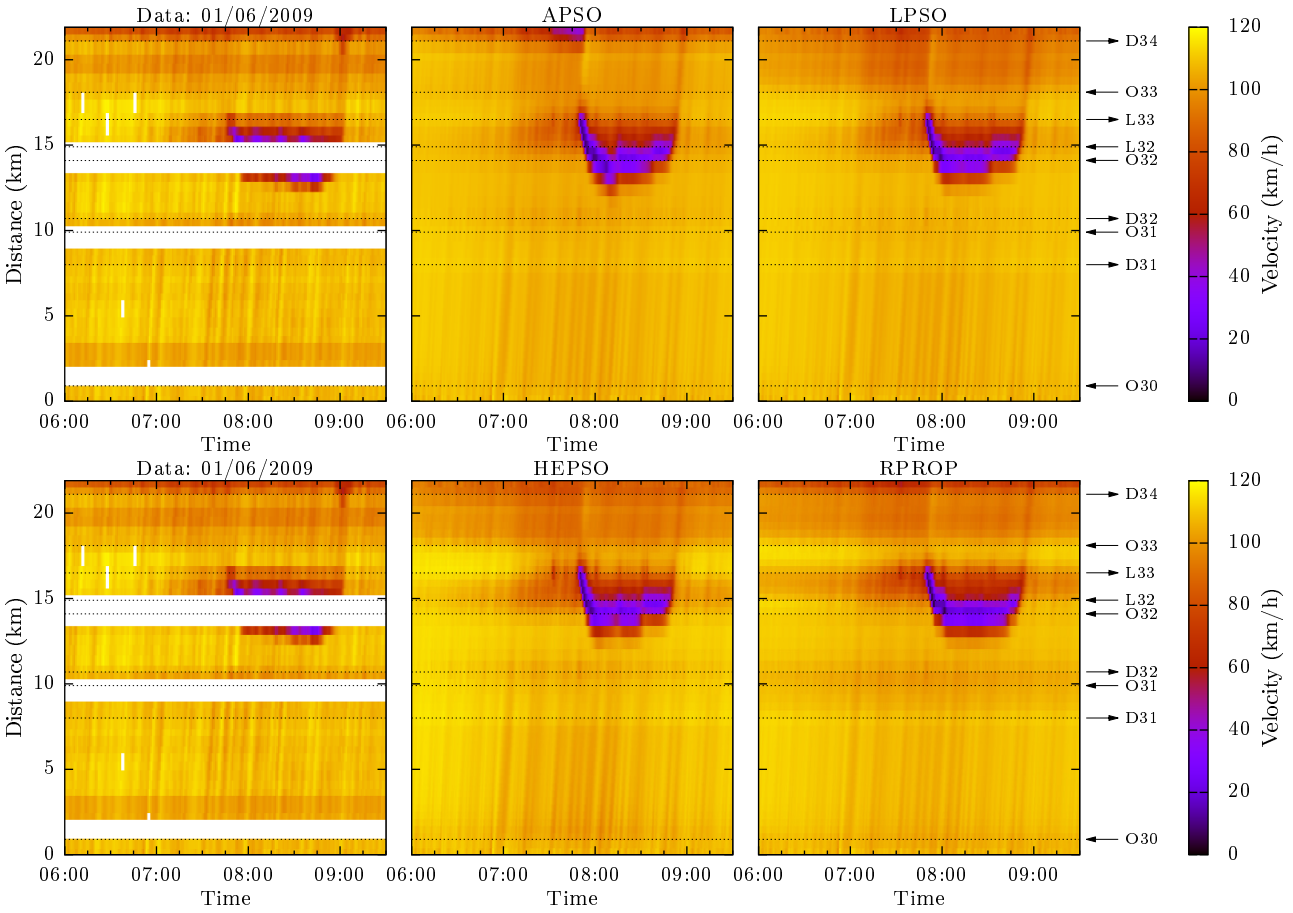

Figure 18: Distance-time diagrams of model output when $\mathbf{z}^*_{15th}$ is applied on the data of the 1st.

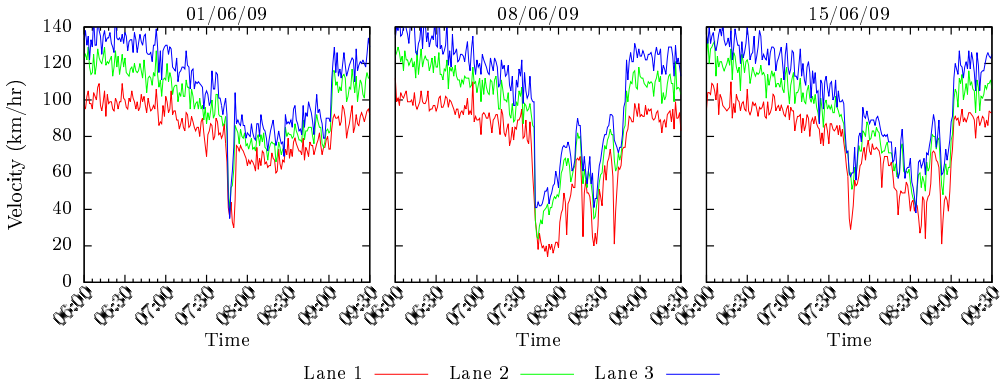

Figure 19: Link L6 lane mean speeds.

List of Tables

Table 1: Traffic flow model parameters upper and lower limits.

Variable	τ	κ	ν	$v_{\min}$	$\rho_{\max}$	δ	ϕ	α_m	$v_{f,m}$	$\rho_{cr,m}$
Maximum	40	30	80	8	190	4	4	3.5	130	45.0
Minimum	1	5	1	0.5	160	5E-5	5E-5	0.5	60	18.0

Table 2: Calibration results for J and J_v.

	Algorithm							
Calibration	**APSO**		**LPSO**		**HEPSO**		**RPROP**	
day & repeat	J	J_v	J	J_v	J	J_v	J	J_v
1st								
Repeat 1	56.54	**55.84**	55.17	**54.20**	66.76	66.00	48.50	39.66
Repeat 2	74.34	73.40	57.51	56.22	54.85	**53.14**	49.21	**36.96**
Repeat 3	59.04	57.93	59.43	58.86	67.33	65.59	51.37	40.47
8th								
Repeat 1	58.67	**55.63**	45.05	42.09	72.70	66.41	43.27	36.96
Repeat 2	59.34	56.21	46.00	42.99	74.41	70.87	42.91	36.55
Repeat 3	58.80	55.94	40.69	**38.36**	78.81	**66.12**	43.36	**36.53**
15th								
Repeat 1	53.22	**51.45**	52.74	51.08	76.48	75.12	52.17	33.73
Repeat 2	57.41	56.49	48.86	**47.62**	65.04	62.51	52.37	**32.13**
Repeat 3	53.31	51.66	51.66	50.13	58.00	**55.36**	62.21	38.92

Table 3: Global parameter set part of the optimal solutions with respect to J_v at Table 2.

Algorithm and day	τ (s)	κ (veh/km/lane)	ν (km^2/h)	v_{min} (km/h)	ρ_{max} (veh/km/lane)	δ (h/km)	ϕ (h/km)
1st							
APSO	34.61976	29.98992	69.29486	0.50681	176.39493	1.22392	0.38401
LPSO	27.18447	24.42183	62.90250	6.07502	163.78077	0.00292	0.97145
HEPSO	25.27353	30.00000	49.95481	0.50000	182.88233	1.21320	0.44915
RPROP	22.66770	22.39974	56.68164	6.17592	182.74620	0.07998	0.00005
Average	27.43636	26.70287	59.70845	3.31444	176.45106	0.63001	0.4511
8th							
APSO	10.01407	22.69213	37.39691	6.94787	171.58465	1.19801	1.13019
LPSO	9.00043	29.99409	37.05295	0.65599	189.80508	0.00012	0.37390
HEPSO	9.64155	15.47807	29.94731	7.71891	166.33726	0.70086	0.00005
RPROP	11.38901	29.17435	41.96460	7.99811	173.29710	0.00008	0.00005
Average	10.01126	24.33466	36.59044	5.83022	175.25602	0.47477	0.37605
15th							
APSO	20.40073	26.02473	41.00612	7.33238	181.03158	0.00017	0.68438
LPSO	20.94335	29.68857	48.24827	5.87563	189.84335	0.00025	0.34124
HEPSO	25.12054	13.15713	41.30585	8.70860	155.08886	0.57899	0.65611
RPROP	18.57291	24.71475	40.34273	8.00000	177.83464	0.09266	0.00005
Average	21.25938	23.39629	42.72574	7.47915	175.94960	0.16802	0.42045

Table 4: Fundamental diagram parameter parts of the optimal solutions for the data set of the 1st.

Algorithm	**FD link start** (name)	**FD link end** (name)	v_f (km/h)	ρ_{cr} (veh/km/lane)	α (–)	**Capacity** (veh/h/lane)
APSO	L1	L7	114.66	24.714	2.677	1951
	L8	L10	107.88	22.574	2.657	1671
	L32	L32	114.57	29.396	2.663	2314
	L33	L33	116.77	30.447	2.681	2449
LPSO	L1	L5	112.21	28.197	2.668	2175
	L6a	L10	111.19	23.967	2.704	1841
	L32	L32	112.90	28.463	2.663	2208
	L33	L33	115.84	32.422	2.736	2606
HEPSO	L1	L7	113.88	25.671	2.609	1993
	L8	L10	106.08	24.256	2.543	1737
	L32	L32	110.88	20.454	2.930	1612
	L33	L33	103.23	27.696	2.650	1960
RPROP	L1	L1	112.71	27.365	2.698	2129
	L2	L2	112.63	28.958	2.683	2247
	L3	L3	108.39	28.165	2.696	2107
	L4	L4	103.60	28.092	2.706	2011
	L5	L5	106.61	28.631	2.717	2112
	L6a	L6a	125.79	23.938	2.702	2080
	L6	L6	113.10	23.510	2.698	1835
	L7	L7	118.38	26.472	2.691	2161
	L8	L8	100.59	26.493	2.690	1838
	L9	L9	113.76	26.508	2.700	2082
	L10	L10	83.51	24.009	2.696	1384
	L32	L32	102.98	25.920	2.696	1842
	L33	L33	125.79	31.860	2.696	2766

Table 5: Fundamental diagram parameter parts of the optimal solutions for the data set of the 8th.

Algorithm	**FD link start** (name)	**FD link end** (name)	v_f (km/h)	ρ_{cr} (veh/km/lane)	α (–)	**Capacity** (veh/h/lane)
APSO	L1	L9	112.23	23.399	2.864	1852
	L10	L10	91.08	24.829	2.724	1567
	L32	L32	115.55	24.264	2.838	1971
	L33	L33	104.55	27.719	3.062	2091
LPSO	L1	L3	112.53	29.889	2.574	2281
	L4	L7	113.50	23.657	2.467	1790
	L8	L9	104.69	27.843	2.446	1937
	L10	L10	90.09	27.265	2.336	1601
	L32	L32	116.99	27.265	2.479	2131
	L33	L33	112.13	25.847	2.625	1980
HEPSO	L1	L2	112.67	35.766	2.275	2596
	L3	L3	111.11	29.986	2.407	2199
	L4	L7	113.71	22.923	2.556	1763
	L8	L10	101.18	31.830	2.274	2075
	L32	L32	107.78	31.362	2.062	2081
	L33	L33	105.37	30.530	2.125	2009
RPROP	L1	L1	116.52	26.531	2.265	1988
	L2	L2	115.52	30.264	2.236	2235
	L3	L3	113.54	27.525	2.252	2004
	L4	L4	109.12	24.626	2.261	1727
	L5	L5	114.99	21.082	2.276	1562
	L6a	L6a	111.42	23.672	2.278	1700
	L6	L6	115.31	23.696	2.285	1764
	L7	L7	117.50	26.335	2.267	1991
	L8	L8	105.29	27.230	2.261	1842
	L9	L9	111.81	28.433	2.260	2042
	L10	L10	83.41	28.078	2.258	1504
	L32	L32	123.15	26.015	2.277	2065
	L33	L33	125.79	26.085	2.279	2116

Table 6: Fundamental diagram parameter parts of the optimal solutions for the data set of the 15th.

Algorithm	**FD link start** (name)	**FD link end** (name)	v_f (km/h)	ρ_{cr} (veh/km/lane)	α (–)	**Capacity** (veh/h/lane)
APSO	L1	L7	112.24	28.155	2.651	2167
	L8	L9	110.47	24.808	2.641	1877
	L10	L10	95.44	23.078	2.448	1464
	L32	L32	113.82	27.641	2.656	2159
	L33	L33	107.41	28.510	2.534	2064
LPSO	L1	L4	111.95	28.376	2.673	2185
	L5	L7	112.17	24.383	2.693	1887
	L8	L10	101.93	23.843	2.645	1665
	L32	L32	111.00	27.813	2.703	2133
	L33	L33	112.17	24.383	2.693	1887
HEPSO	L1	L7	114.91	24.666	2.710	1960
	L8	L10	102.07	25.583	2.682	1799
	L32	L32	115.20	30.074	2.730	2402
	L33	L33	103.97	30.539	2.330	2067
RPROP	L1	L1	114.10	28.843	2.221	2098
	L2	L2	115.76	30.951	2.200	2274
	L3	L3	112.05	28.667	2.212	2044
	L4	L4	108.08	25.811	2.216	1777
	L5	L5	118.44	22.997	2.219	1736
	L6a	L6a	128.23	22.976	2.230	1882
	L6	L6	108.89	26.499	2.252	1851
	L7	L7	119.48	29.163	2.225	2223
	L8	L8	101.22	29.104	2.215	1876
	L9	L9	112.03	29.115	2.214	2076
	L10	L10	80.00	27.140	2.212	1381
	L32	L32	103.81	28.328	2.240	1882
	L33	L33	69.09	36.751	2.231	1622

Table 7: J_v for optimal parameter sets from calibration using data from different dates.

Algorithm	**Calib.**	**Verification date**			
	date	1st	8th	15th	8th (incident)
APSO	1^{st}	55.84	154.98	151.99	88.61
	8^{th}	579.97	55.63	604.04	137.45
	15^{th}	77.83	149.90	51.45	64.38
LPSO	1^{st}	54.20	159.83	155.87	82.76
	8^{th}	826.59	38.36	727.41	140.89
	15^{th}	77.44	155.76	47.62	73.45
HEPSO	1^{st}	53.14	155.81	153.88	85.98
	8^{th}	459.95	66.41	514.61	76.25
	15^{th}	83.07	159.63	55.36	73.87
RPROP	1^{st}	36.96	141.00	106.65	55.66
	8^{th}	338.26	36.55	327.48	103.38
	15^{th}	83.22	140.47	32.13	61.65